CERN-ACC-2021-017

April 28, 2023

Sextupole scheme optimisation for HL–LHC

Fabien Plassard[*]*, Riccardo De Maria, Massimo Giovannozzi*
CERN, CH-1211 Geneva, Switzerland

Abstract

One essential upgrade of the High Luminosity LHC (HL–LHC [1]) to reach the desired luminosity, is the large reduction of the β-function value at the interaction points (IP) hosting the high-luminosity experiments ATLAS and CMS. The achromatic telescopic squeeze (ATS [2]) approach has been adopted for HL–LHC, to overcome various limitations stemming from the ring quadrupoles and sextupoles when the β function at the IP is strongly reduced. The resulting large β waves at the sextupole locations excite strong non-linearities that are compensated in the baseline design by adding four sextupoles to the regular part of the magnetic lattice. This avoids life-time losses due to a reduction of the dynamic aperture (DA). In this study, alternative sextupole correction schemes are proposed and compared with the baseline. These schemes have the advantage of avoiding the costly and time-consuming installation of the additional sextupoles, while keeping the DA at the required level and the optics parameters within the constraints. The optimisation process and the impact on the linear optics, aberrations, and dynamic aperture are summarized and discussed in this report.

Keywords

HL–LHC, dynamic aperture, resonant driving terms, lattice optimisation

[*]fabien.plassard@cern.ch

Contents

1 Introduction

The design upgrade towards the High Luminosity LHC (HL–LHC) foresees to push the parameters of the LHC beam and the ring optics [1] to enable the machine to deliver an integrated luminosity of at least 250 fb^{-1} per year in the two high-luminosity collision points IP1 and IP5 hosting the detectors ATLAS and CMS, respectively. One essential upgrade to reach the desired HL–LHC performance is the reduction of the transverse beam size at the IP, which requires squeezing down β^*. To overcome various limitations stemming from the ring quadrupoles and sextupoles to reduce to very low values β^*, a novel approach to the squeeze of β^*, named achromatic telescopic squeeze (ATS) [2], has been developed and adopted for the HL–LHC.

The reduction of the β-functions at the IPs from the pre-squeeze value of β^* of 50 cm towards the nominal squeeze β^* of 15 cm, for the round optics, is performed by varying the matching quadrupole strengths located in the Insertion Regions IR8/2 and IR4/6 adjacent to IP1 and IP5, respectively. The resulting β-beating waves in sectors 45, 56, 81 and 12 contribute to the β^* squeeze while keeping the quadrupole strengths of the high-luminosity insertions constant. Furthermore, thanks to a proper phasing of the arc cell, a stable chromatic correction is performed, with the strength of the lattice sextupoles nearly constant. In each arc, half of the chromatic sextupoles are called strong: they are in phase with the triplet and used for chromatic corrections, i.e. chromaticity, off-momentum β-beating and dispersion, generated by the triplets as well as by the arcs. The increase of the peak $\beta_{x,y}$ at the strong sextupoles in the arcs during the squeeze excites sextupolar resonant driving terms (RDT) that rise with the so-called ATS factor, i.e. the ratio between the pre-squeeze β^* and the squeeze β^*. If they are left uncompensated, these aberrations induce tune spread that can reduce the dynamic aperture (DA), i.e. the region of phase space where particles survive after a given number of turns, and therefore the beam lifetime. Within each arc adjacent to IP1 and IP5, the non-linear kick generated by the strong sextupoles can be compensated, at the lowest order, when pairs of sextupoles are separated by a phase advance of π. Therefore, a self-compensation of the aberrations excited during the ATS process can be obtained if each circuit of strong sextupole contains an even number of magnets.

In the current LHC lattice, there are 9 and 11 strong sextupoles in the arc 81 and 45 for Beam 1 (arc 12 and 56 for Beam 2), respectively. Consequently, the HL–LHC optics baseline envisages the installation of an additional sextupole, named MS10, at the quadrupole Q10 in the IR1 and IR5 dispersion suppressor. The additional MS10 has a positive impact on the DA and has also the advantage of reducing the excitation level required for the strong sextupoles, which is one of the limiting factor of the smallest β^* attainable without mismatching the arc.

Section 2 first recalls the impact of these additional sextupoles on RDTs and DA. Alternative sextupole layouts and optics have been studied and can restore self-compensation of the non-linear resonances to the same level as the baseline optics, but without MS10. These lattices have the advantage of avoiding the time-consuming interventions for the installation of the needed additional sextupoles. The optics changes and performance of these alternative designs are discussed in Section 3 and follow the studies started in [3–5]. The final performance of the different proposed optics are detailed in Section 3.2 where the phase advances between the two low-β^* IPs are tuned to increase the DA. Numerical simulations are based on the latest version of the HL–LHC layout. The layout and optics of HL–LHC has evolved continuously in the past years since its first version, HLLHCV1.0 [6, 7]. These changes result from performance updates, cost optimisation, hardware development, new request from experiments, and experience gained during LHC Run 2 [8–10]. The optics version used for the studies reported in this article is HLLHCV1.4, on which the proposed changes have been encapsulated in [11–13].

2 MS10 sextupole for HL–LHC: aberrations and long-term stability

Several lattice sextupole schemes, designed to keep the ring DA at a viable level, has been proposed already in past studies [2–5]. The following presents a detailed, quantitative comparison of the perfor-

Table 1: Sextupole circuits (listed by category - the number of magnets in each circuit is reported in parentheses) correcting chromaticity, off-momentum β-beating and dispersion generated in IR1 and IR5. Strong circuits are in phase with the triplet in IR1 and IR5 and used to correct for chromatic errors generated by the triplet and approximately by half of the overall chromatic errors generated by the quadrupoles in the beta-beating sectors (12, 45, 56, 81). Local sextupoles only correct the natural chromaticity of the remaining quadrupoles in the beta-beating sectors. Weak circuits, not indicated in the table, compensate chromaticity generated in remaining sectors (23, 34, 67, 78) and are used to tune the machine chromaticity.

No MS10 circuit	Baseline circuit	Sectors	Beam	Category
SF1 (**9**) , SD2 (**12**)	SF1 (**10**), SD2 (**12**)	81, 45	B1	Strong
SF1 (**10**), SD2 (**11**)	SF1 (**10**), SD2 (**12**)	12, 56	B1	Strong
SF2 (**10**), SD1 (**11**)	SF2 (**10**), SD1 (**12**)	81, 45	B2	Strong
SF2 (**9**) , SD1 (**12**)	SF2 (**10**), SD1 (**12**)	12, 56	B2	Strong
SF2 (**10**), SD1 (**12**)	SF2 (**10**), SD1 (**12**)	81, 45	B1	Local
SF2 (**10**), SD1 (**12**)	SF2 (**10**), SD1 (**12**)	12, 56	B1	Local
SF1 (**10**), SD2 (**12**)	SF1 (**10**), SD2 (**12**)	81, 45	B2	Local
SF1 (**10**), SD2 (**12**)	SF1 (**10**), SD2 (**12**)	12, 56	B2	Local

mance expected for the HL–LHC baseline optics and the LHC-like configuration, which features an odd number of strong sextupoles in the arcs neighbouring IR1 and IR5 insertions. The considerations made are based on non-linear resonances, tune footprints, and long-term stability of the beam.

2.1 Lattice sextupole powering scheme

The strong sextupoles are located in sectors 81, 12, 45, 56 where the β-beating waves reach their maxima. They are responsible for the full correction of the natural chromaticity generated by the triplets and for half of the correction of the natural chromaticity generated by the quadrupoles located in the β-beating sectors. The remaining chromaticity is compensated by the local sextupole family. The LHC-like sextupole lattice, which is here referred to as the *No MS10 optics*, features an odd number of focusing and defocusing strong sextupoles, as detailed in Table 1. For the current *Baseline optics* of the HL–LHC, new focusing and defocusing strong sextupoles, named *MS10F* and *MS10D*, respectively, will be installed at Q10. Figure 1 shows the arrangement of the sextupoles and the $\beta_{x,y}$ functions in sectors 45 and 56 around IP5 (similar configuration for sectors 81 and 12 around IP1). The location of the new MS10F and MS10D for the Baseline optics are indicated in blue in Fig 1.

2.2 Geometrical Resonant Driving Terms and Footprint comparison

The horizontal and vertical betatron phase advances of the arcs are matched to $\Delta\mu_{x,y} = \pi$ between two consecutive focusing (or defocusing) strong sextupoles. Thanks to the design π phase advance, the equal strength and $\beta_{x,y}$ within these pairs of sextupoles (except for the sextupoles in the dispersion suppressor with slightly perturbed β-functions), one obtains a full two-by-two cancellation of the non-linear kicks generated by each strong sextupole. If one strong sextupole is not paired (odd number of magnets), as for the No MS10 optics, its uncompensated sextupole field will propagate through the ring. Figure 2 shows the cumulative sum as a function of s of the main sextupolar geometrical aberrations for the Baseline and No MS10 optics at $\beta^*_{x,y}$ = 15 cm.

The amplitude build-up of the normal geometrical Hamiltonian driving terms generated by the sextupole were computed from the Twiss functions using

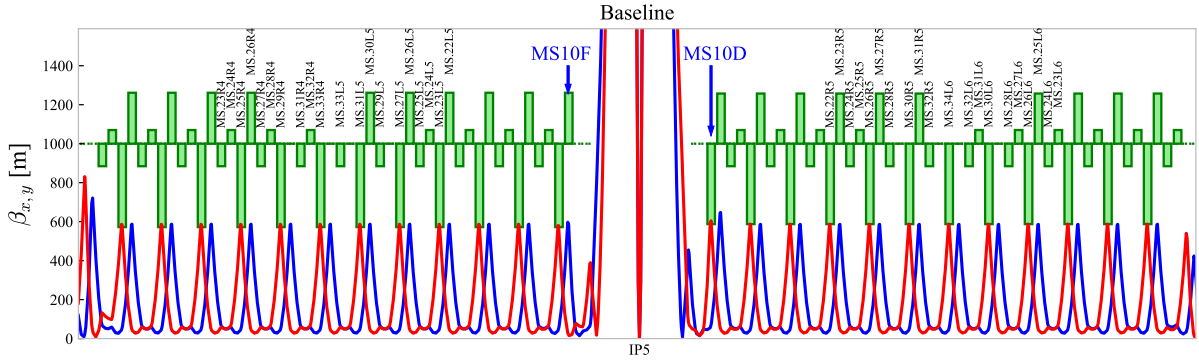

Fig. 1: Sextupole strengths (green boxes in arbitrary units) around IP5 for Beam 1 of the Baseline optics for HL–LHC with the additional focusing and defocusing strong sextupoles MS10F and MS10D (labelled in blue). The focusing/defocusing sextupoles have positive/negative strengths. The strong sextupoles have the largest strength in absolute value, conversely the local ones have the smaller strengths. The β-functions (blue lines for the horizontal plane and red lines for the vertical plane) show how the peak of the beta-beating is located in correspondence to the strong sextupoles. The optics functions and sextupole powering are similar around IP1. The names, as indicated in the LHC lattice repository, of some local and strong sextupoles in the right and left side of IP4, IP5 or IP6 denoted by *R4, L5, R5, L6*, are also shown for reference.

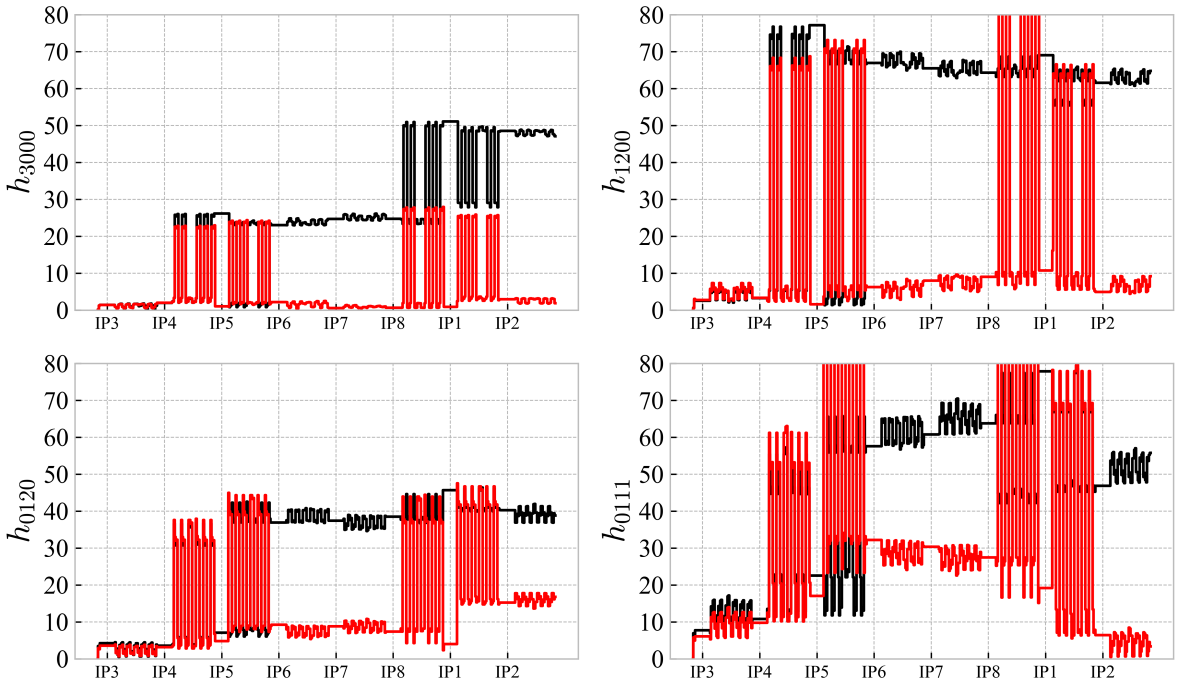

Fig. 2: Main Sextupole geometrical RDTs build-up along the ring with (Baseline optics, red lines) and without additional MS10 (black lines) used for the self-compensation of sextupolar resonances, computed using Eq. (1).

.

$$h_{jklm}(s) = \frac{1}{j!k!l!m!2^{j+k+l+m}} \int_s^{s+L} K_3(s')\beta_x^{\frac{j+k}{2}}(s')\beta_y^{\frac{l+m}{2}}(s')e^{i[(j-k)\Delta\mu_x(s')+(l-m)\Delta\mu_y(s')]}\mathrm{d}s', \quad (1)$$

where K_3 is the integrated strength of the normal sextupole component at location s' and $\Delta\mu_{x,y}$ represents the difference in phase advance between location s' and s. The contribution of the multipoles is of the order $n = 3 = j+k+l+m$, giving rise to terms in the Hamiltonian $\propto x^{j+k}y^{l+m}$ and drive different betatron resonances characterized by ν_x, $3\nu_x$, ν_x-$2\nu_y$, ν_x+$2\nu_y$.

It is clear that restoring the pairs in the chain of the strong sextupoles allows a good control of these RDTs along the ring, which are enhanced with the ATS factor.

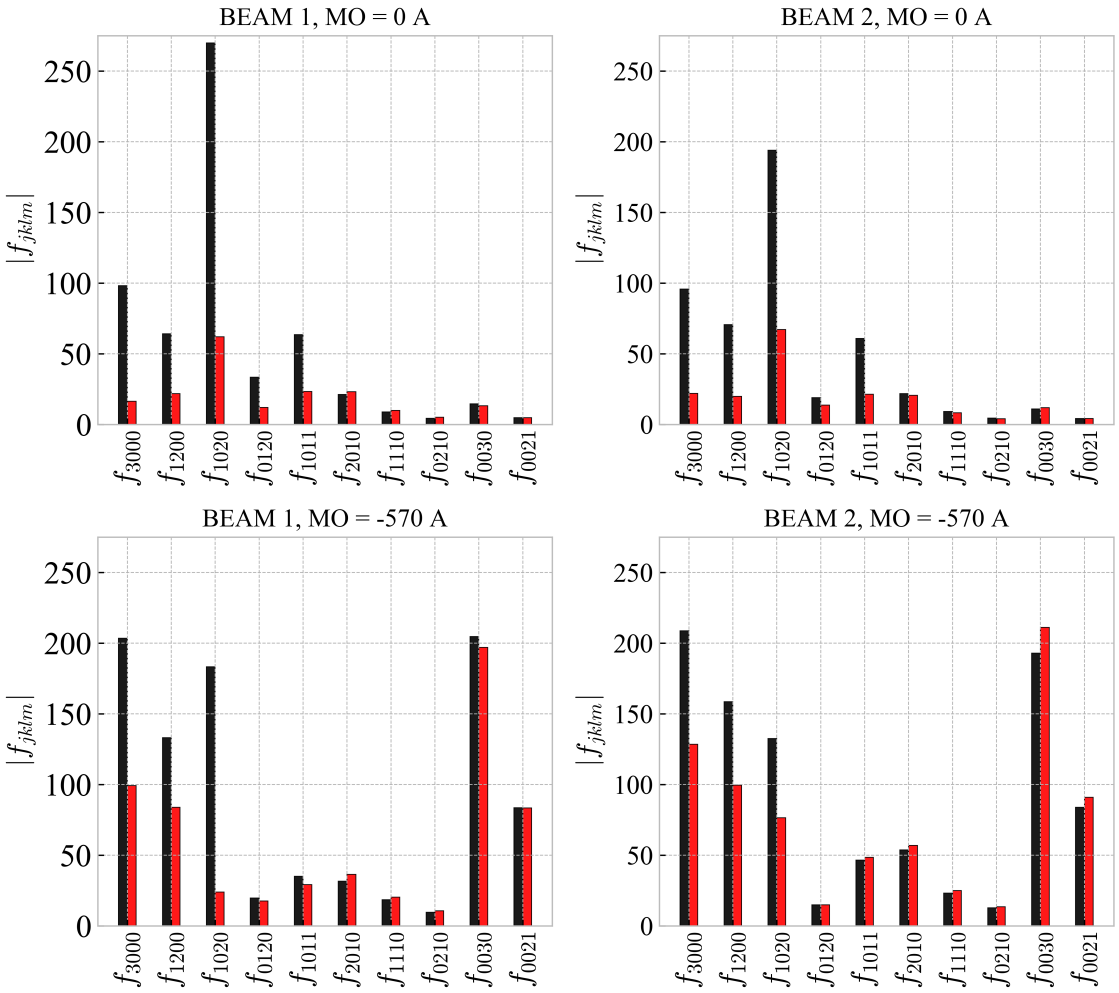

Fig. 3: Average amplitude over each magnetic element of the ring, of the sextupole RDTs coefficient of the normal form (f_{jklm}) for the Baseline (red lines) and No MS10 (black lines) computed with PTC without (top) and with (bottom) Landau octupoles, for both beams. The coefficients f_{jklm} are related to h_{jklm} by $f_{jklm} = h_{jklm} / (1 - e^{i2\pi[(j-k)Q_x + (l-m)Q_y]})$.

Figure 3 shows the average amplitude of the normal and skew terms of order $n = 3$ over the HL–LHC lattice for both optics and beams, computed with PTC [15, 16]. It shows the different sextupolar RDTs calculated by tracking the beam using the HL–LHC crossing scheme in all IPs, as defined in (see Section 2.3), with the orbit bumps of the dispersion correction and compares the situation for the Landau octupoles turned off and switched on to their maximum strength of $I_{\mathrm{MO}} = -570$ A. In all cases, the normal terms of the geometrical aberrations are significantly larger for the No MS10 optics compared with the one with the additional sextupoles. The tune shift induced by these uncorrected aberrations limits the region of phase space where the particles are stable. To map the unstable zones tracing the limits of the dynamic aperture, a Frequency Map Analysis (FMA) [17] has been performed for the two schemes,

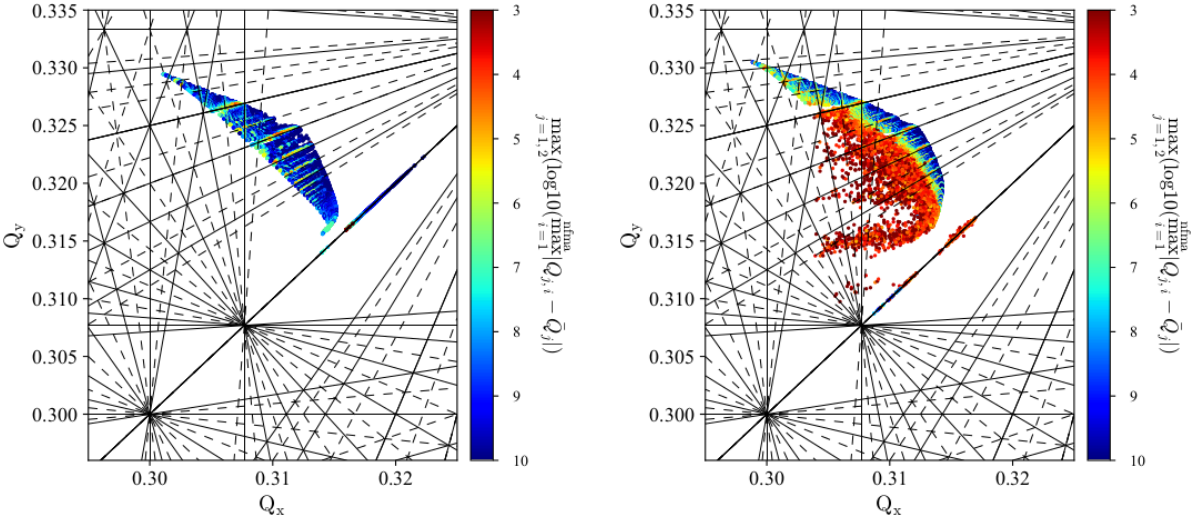

Fig. 4: Frequency Map Analysis for Beam 1 for the Baseline optics (left) and the No MS10 optics (right). Simulations performed at 10σ, 10000 turns, $\delta_p = 2.7\times10^{-4}$, $I_{\mathrm{MO}} = -570$ A, crossing scheme in all IPs defined in Section 2.3, and dispersion correction orbit bumps. The colour scale represents the diffusion in tune in log scale. A moving window FFT is performed to determine the diffusion in tune as defined in [14]. The footprint and the tune diffusion level are large for the No MS10 scenario, compared to the Baseline.

as shown in Fig. 4. The particles were tracked up to 10σ amplitude over 10000 turns, using the nominal working point ($Q_x = 62.31$, $Q_y = 60.32$), with dispersion correction orbit bumps, Landau octupoles and without magnetic field errors. The colour map indicates the tune diffusion rate, used to characterize the stability of the particles, and is calculated as the tune variation between the first and second 5000 turns. The No MS10 scheme generates a larger tune footprint and diffusion rate as compared to the Baseline for similar amplitude values. The chromatic RDTs are very similar among these schemes, which indicates that the larger tune diffusion rate observed for the No MS10 is dominated by the sextupolar geometrical aberrations. The resulting reduction in DA is discussed in the following section.

2.3 Impact on DA

The dynamic aperture was simulated using the tracking code SixTrack [18, 19] and its running environment SixDesk [20] for large numerical simulations. The DA results are compared here between the LHC-like sextupole lattice and the Baseline optics for HL–LHC. The tracking conditions assumed for the simulations are as follows:

- HLLHCV1.4 optics version at collision energy of 7 TeV with round optics, $\beta^*_{x,y} = 15$ cm
- Tunes $Q_x = 62.31$ and $Q_y = 60.32$
- 30 particle pairs per 2σ amplitude step tracked over 10^5 turns
- 7 $x - y$ phase-space angles
- chromaticity of 15 units and an energy spread $\delta p/p$ of 2.7×10^{-4}
- normalized emittance $\epsilon_n = 2.5\mu$m
- half crossing angle $\theta/2$ at IP1/2/5/8 of 295/170/295/-250 μrad
- half parallel separation at IP1/2/5/8 of 0.75/2/0.75/-2
- Landau octupole strengths $I_{\mathrm{MO}} = -570$ A (maximum strength)

– No Beam-Beam effects.
– 60 random error seeds for the generation of magnetic field errors.

The value of the half crossing angle for Point 1 and 5 has been chosen to be the same of the value used for orbit correction budget calculation (295 μrad) [21,22] instead of (250 μrad) as of the operational scenario [23] as a conservative choice since the effect under study depends on the amplitude of the orbit correction bump to correct dispersion that scales with the crossing angle in Point 1 and 5.

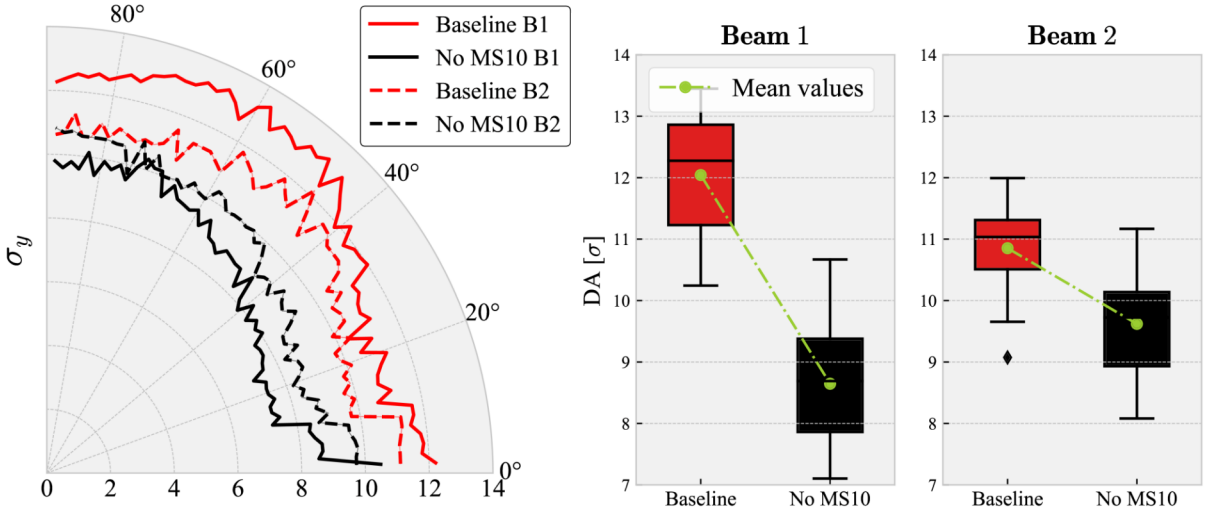

Fig. 5: Dynamic aperture comparison between the Baseline and the No MS10 optics without imperfections. The plots show the angular distribution of the dynamic aperture in the (σ_x,σ_y) plane [24].

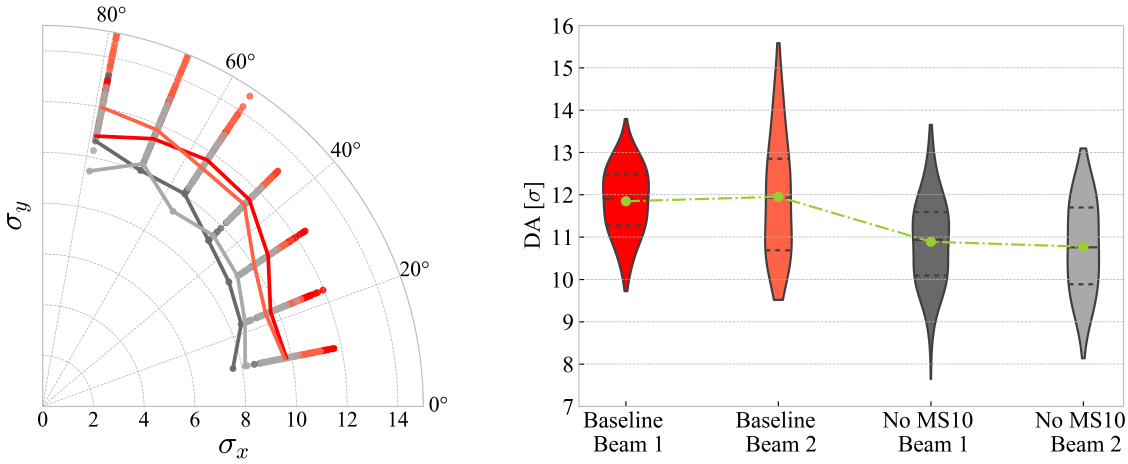

Fig. 6: Dynamic aperture comparison between the Baseline and the No MS10 optics. The left plot shows the spread of the 60 seeds simulated at each of the 7 angles examined in the (σ_x,σ_y) plane, where the solid lines indicate the minimum DA. The right plot shows the distribution of the 60×7 DA results, where the middle black dash line is the median DA and the adjacent dash lines show the interquartile range. The green line and markers show the average DA.

The non-linear field errors included in the tracking are based on the measured field quality of the LHC magnets and estimations for the field quality of the new inner triplet quadrupoles (IT), the D1 and D2 separation dipoles, and the LHC Q4 and Q5 matching quadrupoles. The error tables used for the DA simulations can be found in the HL–LHC repository [25]. After applying these imperfections, linear

optics corrections are applied to rematch the tune, chromaticity, linear coupling and closed orbit, as well as non-linear correction of the multipolar errors of the main dipoles and triplets, D1 of IR1 and IR5, using the spool pieces and the corrector package magnets, respectively. These simulation conditions, unless stated otherwise, are conserved for all DA results on the different optics options presented throughout this report.

The impact on DA of the correction of the geometrical aberrations provided by the MS10 is large even on an error-free machine. Simulations on the No MS10 optics have shown a drop of DA of up to 3 σ after 10^6 turns for the average and minimum DA when no imperfections are applied (see Figure 5). Figure 6 shows the DA results, considering operational conditions and non-linear field errors over 60 seeds (tracked over 10^5 turns). Here, the average DA (DA_{avg}) or the minimum DA (DA_{min}) are defined as the average or minimum over the 7 phase-space angles and over all seeds when imperfections are applied. For the Baseline, $DA_{avg/min}$ = 11.9 / 9.7 σ for Beam 1 and $DA_{avg/min}$ = 12.0 / 9.5 σ for Beam 2. While for the LHC-like sextupole scheme, $DA_{avg/min}$ = 10.9 / 7.6 σ for Beam 1 and $DA_{avg/min}$ = 10.8 / 8.1 σ for Beam 2. Similar important DA differences between the Baseline and No MS10 optics were observed for different tracking setup [26]: with/without dispersion orbit bumps for the spurious dispersion correction, with/without Landau octupoles and with/without energy off-set. The latter allows discarding chromatic contributions as culprit of the DA reduction, and to confirm the dominant impact of the sextupole geometrical aberrations. Alternative sextupole schemes and optics designs were studied and are discussed in detail in Section 3 to assess whether the installation of the additional MS10 sextupoles can be avoided while providing similar cancellation of the RDTs that have strong detrimental impact on DA.

3 Alternative sextupole schemes and optics optimisation without MS10

The installation of the 8 additional MS10 sextupoles (for Beam 1 and 2), part of the HL–LHC baseline since the beginning of the project, implies several efforts and a complex logistic. To alleviate these long and costly interventions, two new sextupole layouts (labelled *No MS14F* and *No MS14F & MS14D* respectively) were proposed and are discussed in this section.

3.1 Sextupole layout and optics changes

The first alternative option for the HL–LHC sextupole scheme without MS10 has been proposed and studied in the past in [3–5]. As previously discussed, the sextupole scheme needs to self-compensate the sextupolar fields that deteriorate the DA. This can be achieved by restoring an even number of magnets in the strong sextupole family circuits around IP1 and IP5. The strategy adopted for the first option was to bypass the strong sextupoles, named MS14F.R8 and MS14F.R4 on the left side of IP1 and IP5, respectively, for the Beam 1 and the MS14F.L2 / MS14F.L6 for Beam 2, where the horizontal β_x waves are close to their maximum peak. Thanks to the available margin in the strength of these focusing sextupoles, the remaining 8 magnets can compensate the disconnected MS14F for chromatic correction while keeping the required margin. The bypass of the MS14F induces an increase in the strength of the focusing sextupoles of around 10%. Instead of disconnecting the MS14F close to Point 8/4 for Beam 1 and in Point 2/6 for Beam 2, one could also bypass the MS14F close to Point 1/5 to obtain an even number of magnets. However, one has to consider the orbit bumps generated for dispersion correction in IP1/5. The horizontal orbit bump is designed to reach the peak orbit at the location of an even number of strong sextupoles to cancel the induced feed-down generating β-beating. Unlike the former option, the MS14F close to Point 1/5 are located at a peak of an orbit bump. If these magnets are disconnected, the compensation of these quadrupole fields is broken and results in a leak of β-beating of more than 10% along the ring, as shown in Fig. 7.

The same is true for the vertical orbit bumps, where uncompensated feed-down to skew quadrupole field would generate linear coupling. This option was therefore discarded.

Since the defocusing sextupoles require larger excitation level and to obtain an even number of

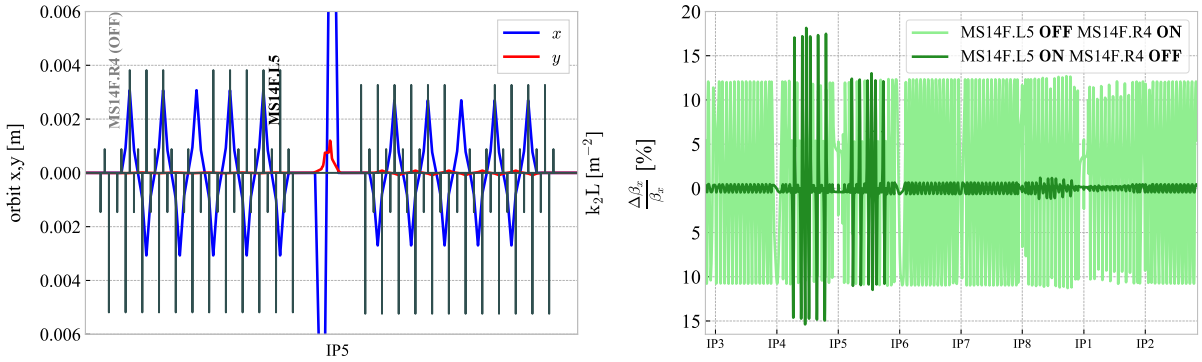

Fig. 7: Left: orbit with crossing angle at IP5 and dispersion correction bumps. The sextupole scheme of the No MS14F optics, with the magnet in IR4 disconnected, is shown by the black lines. Right: β-beating along the HL–LHC if the MS14F in IR5 is disconnected (light green line) and when the one in IR4 is disconnected (dark green line).

strong sextupoles on the right side of IP1/5, a different strategy than bypassing another magnet has been adopted. As shown in Table 1, in the current LHC configuration there are on the right side, 11 strong defocusing sextupoles and 12 of the local family. By shifting the vertical betatron phase by $\Delta\mu_y = -\pi/2$ in sector 12 and 56, the β_y peaks will be reached at the 12 former local family sextupoles. The MS14F bypass, the vertical phase shift, and the inversion between the defocusing strong and local families in sector 12 and 56, allow restoring the pairing of the strong sextupoles in IR1/5. It is worth mentioning, that the betatron phase shift of $-\pi/2$ is a delicate optics exercise due to the constraints on magnets, experiment, machine protection and has to allow safe squeeze optics. The latter has been verified by optimizing the squeeze optics from injection to collision [27]. Also, the strong sextupoles are used for the correction of the spurious dispersion generated by the orbit excursion at the triplet quadrupoles from the crossing scheme.

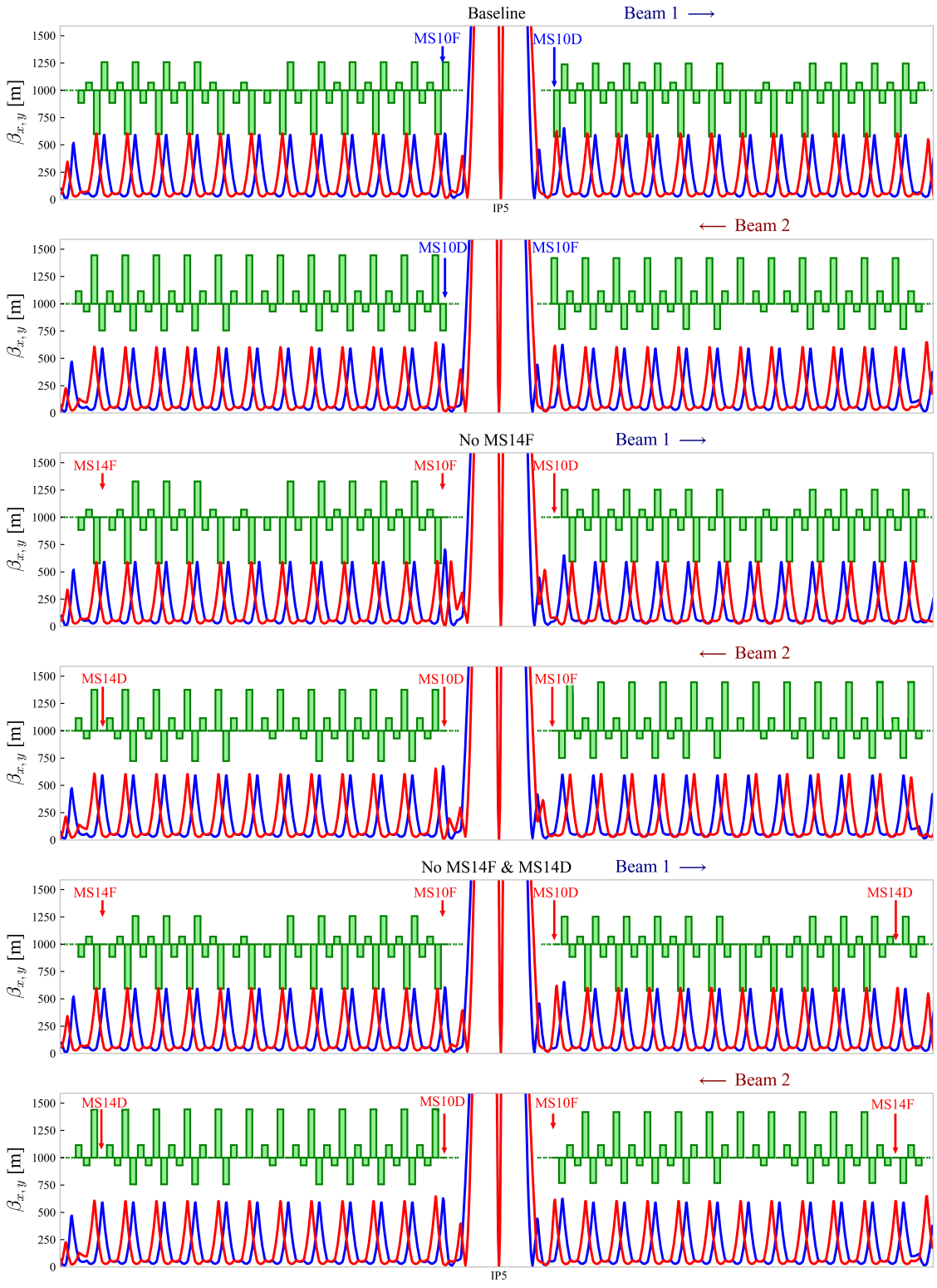

Fig. 8: Lattice sextupole configuration around IR1 of the Baseline, the No MS14F and the No MS14F & MS14D optics. The sextupoles annotated in red are removed in the scheme compared to the Baseline lattice, and in blue are the additional sextupoles compared to the current LHC configuration. The naming of *MS14F* and *MS14D*, referring to the different optics options mentioned in this report, are based on Beam 1 sextupole scheme. For Beam 2, the focusing and defocusing sextupoles are inverted as shown here.

Orbit bumps are generated by dipole correctors at the strong sextupole locations to generate dispersion beating waves that will compensate the spurious dispersion. Due to the shift of vertical phase, the dispersion correction knobs were also changed by shifting the orbit bumps to provide equivalent correction as the baseline. Optics-wise, this alternative optics fulfils all the machine constraints. The layout of this option, here referred to as *No M14F optics*, is shown in the middle plot of Fig. 8.

The second design option proposes a simpler strategy, which does not require important changes to the optics, such as large betatron phase shift. The left side of IP1/5 is similar, as for the first option: bypass the MS14F in IR8/IR4. On the right side, the vertical phase is kept unchanged, but the strong defocusing sextupoles MS14D in IR2 and IR6 are disconnected. This option will be referred to as *No MS14F* and *MS14D optics*, and its scheme is shown in the bottom plot of Fig. 8. The main drawback of this configuration is the reduction of strength of the strong sextupole family for chromaticity compensation by $\approx 20\%$ compared to the HL-LHC sextupole configuration. The missing strength is compensated by the arc sextupoles in sectors 23,34,67 and 78. As discussed later, this compensation leads to a slight increase in the vertical chromatic β-beating in IR6, IR3 and IR7, which host the dump and collimation systems. This option needs to be studied from a machine protection and collimation point of view to assess its feasibility, as there are no specifications on the maximum tolerated off-momentum beta-beating.

3.1.1 Properties of the new schemes

As a result of the changes done in the IR1/5 sextupole circuits for the *No MS14F* and *No MS14F & MS14D optics* optics, the sextupolar geometrical aberrations are now well compensated by design. The first-order value of the driving terms h_{1200}, h_{3000}, h_{1011} and h_{1020} are shown in Fig. 9 and present similar compensation as for the Baseline, without the need of additional magnets.

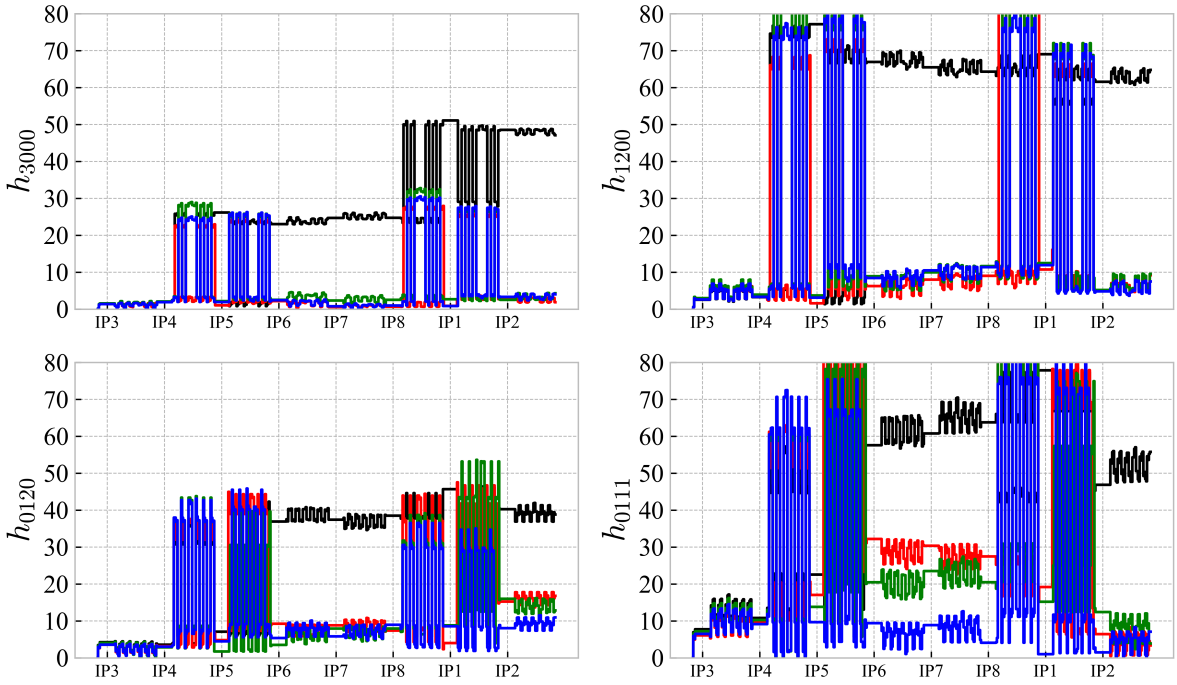

Fig. 9: Comparison of the sextupole geometrical RDTs build-up along the ring for the *No MS10* (black lines), *Baseline* (red lines), *No MS14F* (green lines) and *No MS14F & MS14D optics* (blue lines) optics.

In operation, the machine needs octupoles to generate spread of betatron tunes, effective at small amplitudes, for the stability of the collective motion of the bunched particles (Landau damping). Experience from LHC operations shows that the HL–LHC might require a factor 2 stronger Landau octupoles

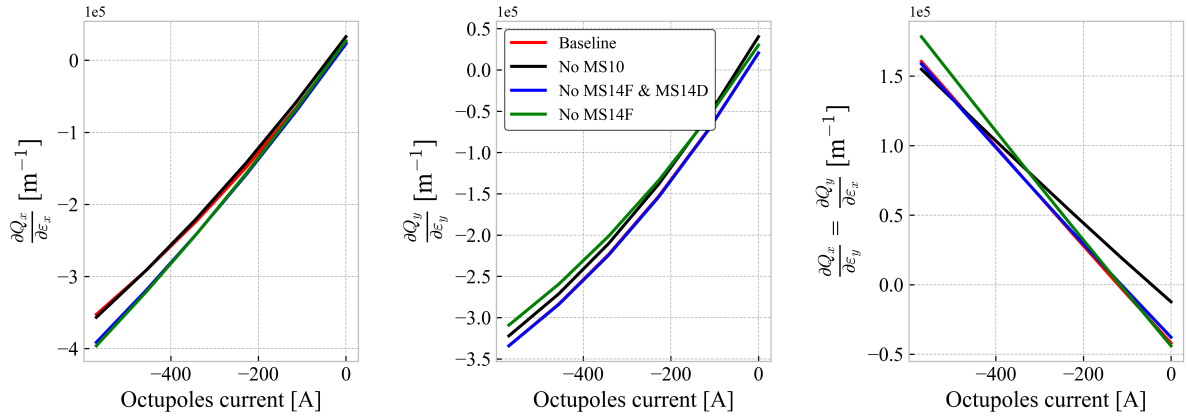

Fig. 10: Linear amplitude detuning terms as a function of Landau octupole current for the Baseline, No MS10, No MS14F and No MS14F & MS14D optics (Beam 1) when fully squeezed at flat-top energy. The Baseline case is hardly distinguishable from No MS14F & MS14D for $\partial Q_y / \partial \epsilon_y$.

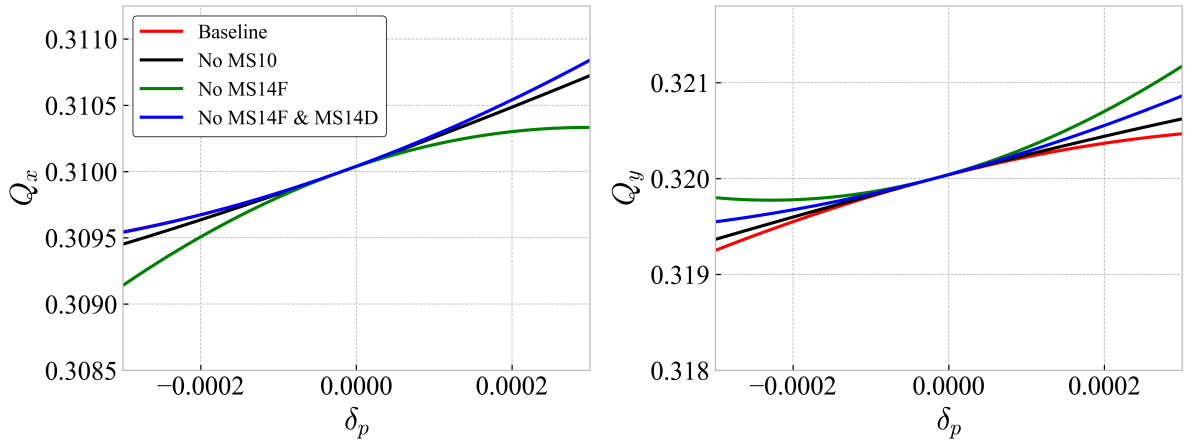

Fig. 11: Tunes versus momentum offset for Beam 1. Without Landau octupoles ($I_{\mathrm{MO}} = 0$ A) when fully squeezed at flat-top energy. The Baseline case is hardly distinguishable from No MS10 for $Q_X(\delta_p)$.

than suggested by simulations, to insure stability [28]. The simulations are thus performed here using the maximum current allowed for the octupoles to check the feasibility of the different designs under pessimistic, but not unrealistic scenarios. Although the octupole circuits did not change between the different proposed optics, one can expect changes in the linear amplitude detuning terms due to the different sextupole lattices and the vertical phase shifts performed on the No MS14F optics. Sextupoles generate second-order contributions to linear amplitude tune shift [29], proportional to K_3^2. The contribution from the main sextupoles only is shown in Fig. 10 for octupoles current set to 0 A. However, this contribution is small compared to the linear amplitude detuning generated by the octupoles. For the No MS14F optics, the vertical betatron phase shift results in loosing a peak of β_y at a Landau octupole in IR2 and IR6. Therefore, two octupoles will have almost no contribution in the generation of vertical tune spread ΔQ_y. Furthermore, the phase shift performed on No MS14F optics has changed the betatron amplitude conditions at the location of certain octupoles, leading to an increase in the terms proportional to $\beta_x \times \beta_y$, and therefore has increased the amplitude detuning cross terms. It is worth mentioning that in the case of negative current for the Landau octupoles, as considered for fully squeezed HL–LHC operation, the direct terms are the main contributors to the stability [28].

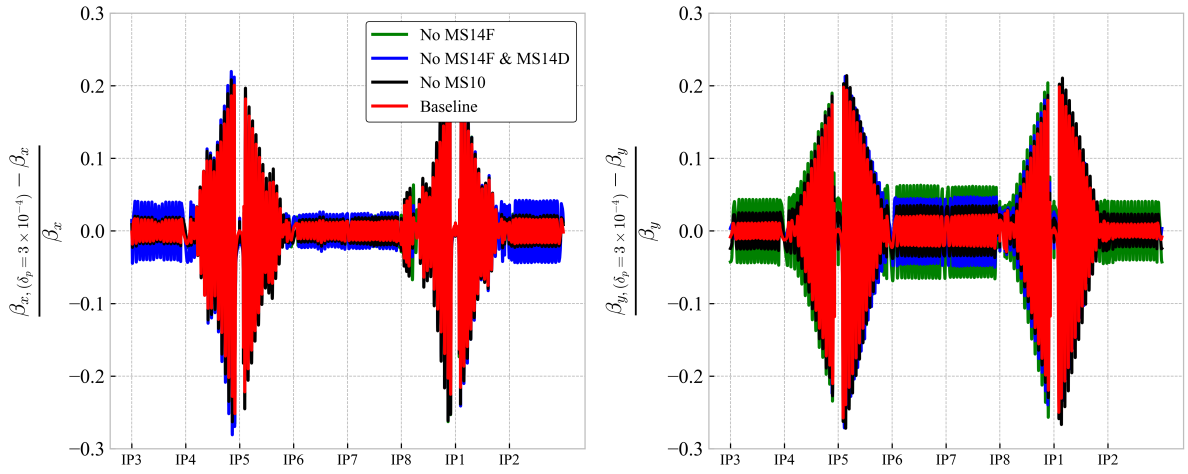

Fig. 12: Amplitude of the chromatic β-beating along the machine for the different sextupole lattice options.

The change of the linear amplitude detuning terms $\partial Q_x/\partial\epsilon_x$, $\partial Q_y/\partial\epsilon_y$, and $\partial Q_y/\partial\epsilon_x$ $(= \partial Q_x/\partial\epsilon_y)$ as a function of the octupole strength, up to their maximum values, is shown in Fig. 10. The quadratic evolution of the linear amplitude detuning terms results from the second-order contributions of the feed-down to sextupolar fields generated by the orbit bumps at the Landau octupoles around IP1 and IP5. The differences in linear amplitude detuning terms between the Baseline optics and the alternatives have a rather small impact on the tune footprint. However, as discussed in Section 3.2, the impact of higher-order detuning terms ($\partial^2 Q_{x,y}/\partial\epsilon^2_{x,y}$, $\partial^3 Q_{x,y}/\partial\epsilon^3_{x,y}$) can be important on the size of the footprint between the different sextupole schemes.

The chromatic behaviour of the machine was also affected by the changes in the sextupole circuits. The chromatic variations of the betatron tunes are essentially linear in a momentum range corresponding to the bucket height ($\delta_p = \pm 4 \times 10^{-4}$), especially for the Baseline and No MS14F & MS14D optics, as shown in Fig. 11. This shows that the non-linear chromaticities Q'' and Q''' are still well minimized. Figure 12 shows the off-momentum β-beating along the ring. As expected from the achromatic design of the HL–LHC optics, the large off-momentum β-beating is confined between the first and last sextupoles located in the arcs participating in the ATS squeeze. The amplitude of the off-momentum β-beating is negligible between the Triplets. By design, the propagation of off-momentum β-beating mitigates any possible deterioration of the physical aperture of the machine.

From Fig. 12, one can observe a leakage of the vertical off-momentum β-beating through the ring. While the beam stay clear, in terms of physical aperture, along the ring for all alternative optics, in the case of the No MS14F & MS14D optics the leakage propagates in the cleaning insertions that impose the most stringent tolerances in terms of β-beating to preserve the collimator hierarchy [30, 31]. For the No MS14F & MS14D optics, there is $\approx 4\%$ β-beating in IR3 which hosts the momentum collimation system, and $\approx 6\%$ β-beating in IR6 and IR7, hosting the dump and betatron collimation systems, respectively. In comparison, the No MS14F and Baseline optics generate a maximum of 2% and 4% β-beating in those insertions, respectively. From the collimation point of view, the No MS14F & MS14D optics should be studied to assess whether one can safely operate the machine with this level of off-momentum β-beating leakage. For all cases, the strong sextupole strength has been limited to 90% of their maximum current (ultimate current). If the limit on the defocusing strong sextupole strength is set to 95% of their maximum current for the No MS14F & MS14D optics, the chromatic β-beating can be reduced to less than 3% in IR3, IR7 and IR6. The impact of pushing the sextupole strength limit to 95% on chromatic β-beating when multipolar field errors are included has been checked and is negligible. The level of chromatic

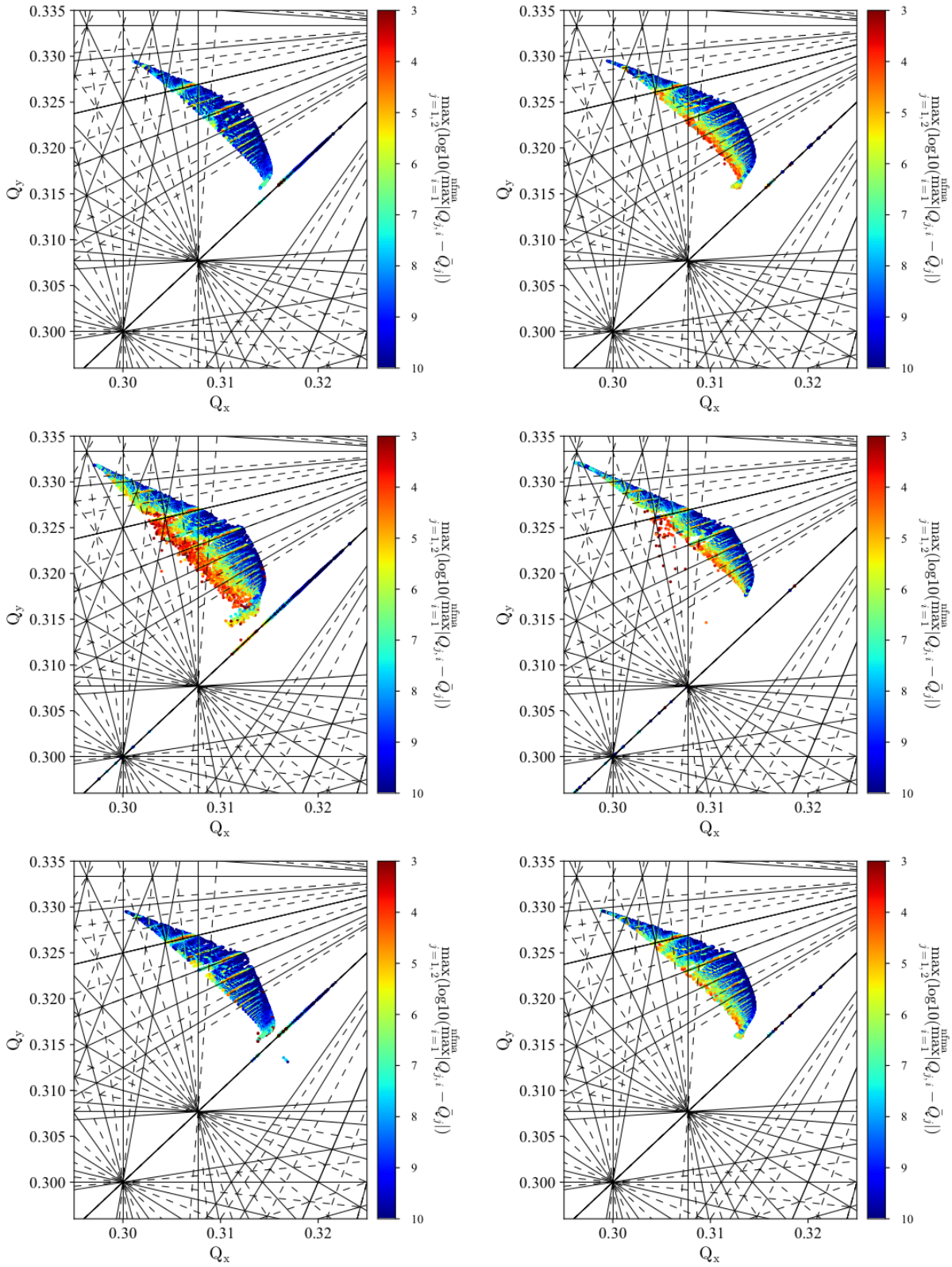

Fig. 13: Frequency Map Analysis on Beam 1 (left plots) and Beam 2 (right plots) for the Baseline (top), No MS14F (middle), and No MS14F & MS14D (bottom) optics.

β-beating stays to $\approx 3\%$ in IR3, IR7 and IR6.

It has been noted in Section 2 that the geometrical aberrations uncompensated by the strong sextupole circuits of the No MS10 optics has a significant impact on the tune footprint and tune diffusion at large amplitudes. Figure 13 shows the FMA simulated up to 10σ with maximum octupole strength, crossing scheme, dispersion correction and with off-momentum beam, for the Baseline (top), No MS14F (middle), and the No MS14F & MS14D (bottom) optics, for Beam 1 and 2. One can observe the clear reduction of the footprint and diffusion level compared to the LHC-like configuration. Concerning the No MS14F optics, there is a sizeable increase in footprint size and tune diffusion for Beam 1 compared to Beam 2 but also the other optics. This was the subject of extensive studies to understand the mechanism behind the observed difference between Beam 1 and Beam 2 that will be detailed in Section 3.2.

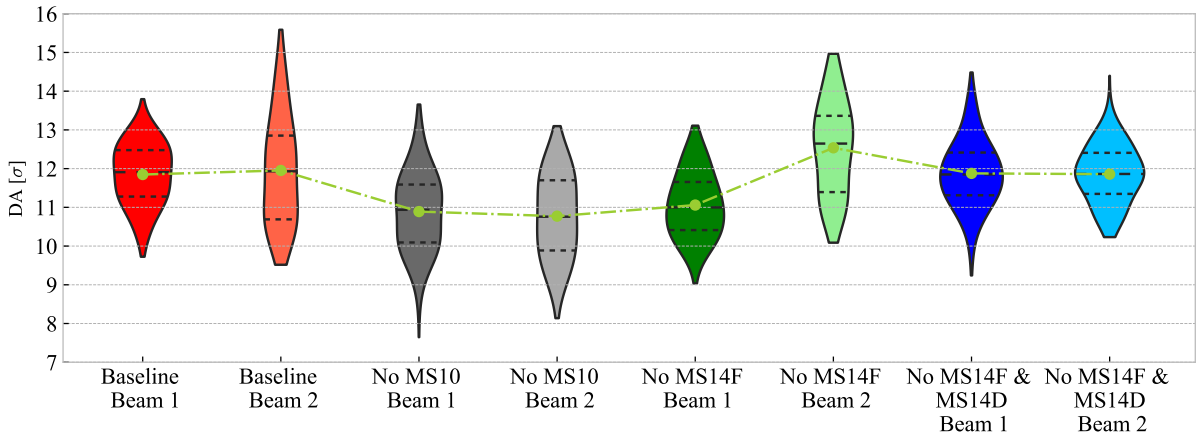

Fig. 14: Dynamic aperture comparison between all optics, with field imperfections and Landau octupoles set to I_{MO} = -570 A.

3.1.2 DA comparison

As an ultimate comparison, Fig. 14 shows the DA simulated with similar setup as stated in Section 2 for all proposed optics and for both beams. In general, the DA is improved for both alternative optics, but, as expected, there is a rather severe drop of DA in average for the Beam 1 of the No MS14F optics compared to the Baseline. For this design, the $DA_{avg/min}$ = 11.1 / 9.1 σ for Beam 1, so $\Delta DA_{avg/min}$ = +0.2/+2.1σ compared to the No MS10 optics. Nevertheless, there is an important improvement of DA for Beam 2, despite the larger spread among the seeds, with $DA_{avg/min}$ = 12.5 / 10.1 σ. For the No MS14F & MS14D case, the $DA_{avg/min}$ = 11.9 / 9.3 σ for Beam 1 and $DA_{avg/min}$ = 11.9 / 10.2 σ for Beam 2, so very similar to the DA computed for the Baseline optics for both beams. Simulations have proven that the DA can be optimized by tuning the phase advance between the two low-β insertions. Especially, difference in DA between Beam 1 and Beam 2 for the No MS14F optics can be considerably reduced with this technique, that will be detailed in the Section.

3.2 Phase advance optimisation between IP1 and IP5

The benefit of optimizing the phase advance between the two low-β insertion points IP1 and IP5 on the minimization of some possible dangerous non-linear terms and ultimately on the DA, has been studied and assessed in the past in [32].

In the present study, one focuses on the compensation of the phase-dependent non-linear perturbations generated by the 'error-free' machine (no non-linear field imperfections included). These non-linear resonances arise from the octupoles, the feed-down fields from the orbit bumps at the multipole magnets and the cross-talk between the various multipolar fields generated by the magnetic errors in the ring.

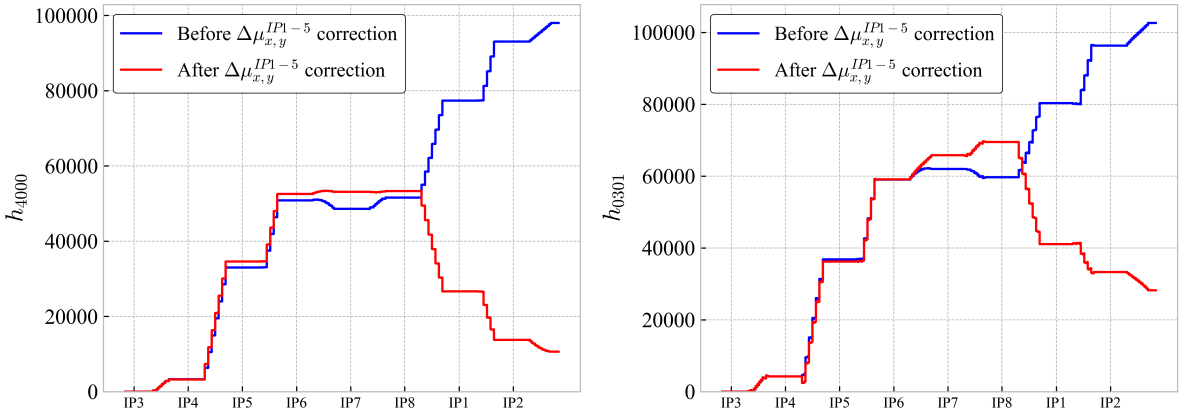

Fig. 15: Example of self-compensation of octupolar RDTs (h_{4000} and h_{0301}) between IR1 and IR5 after $\Delta\mu_{xy}^{IP1-5}$ phase optimisation (Baseline optics).

Therefore, an error-free lattice can generate a wide panel of high-order RDTs, that can deteriorate the DA.

At collision, the large β-functions in the sectors adjacent to IP1 and IP5 (participating in the ATS) where are located the strong sextupoles, the octupoles and the large orbit bumps for dispersion correction, are the main source of high-order RDTs along the ring. Unlike the sextupolar RDTs generated by the strong sextupoles around IP1/5 that are self-compensated by their configuration and phase advance separation, the Landau octupoles however generate octupolar RDTs that grow continuously along the sectors 81,12 around IP1 and along sectors 45,56 around IP5. Higher-order RDTs that take their sources at the octupoles will follow a similar behaviour. Thanks to the similar conditions at IP1 and IP5, the amplitude of the RDTs generated in their neighbouring sectors are also similar, and therefore, one can adjust the phase between these two regions, by adjusting the phase advance between IP1 and IP5 ($\Delta\mu_{xy}^{IP1-5}$), to reverse the direction of the resonances build-up as shown as example in Fig. 15. The difficulty of this optimisation is that the optimal phase separation depends on the nature and order of the perturbation. Due to the complex mechanism behind the source of DA reduction, the scan of $\Delta\mu_{xy}^{IP1-5}$ has been performed by targeting the maximum DA, instead of some possible dangerous resonances.

The phase is changed by using the trim quadrupoles in arcs 23, 34, 67, 78 then re-matching the optics of the ring, and can have implications in those sectors that need to be checked. Especially, the phase constraints from machine protection considerations need to be considered to propose optimized optics that can be safely used during operation. In our study, the constraints imposed by the dump systems were included to draw limitations in the $\Delta\mu_{xy}^{IP1-5}$ scan performed on the different sextupole lattice designs. The main constraint is the phase advance from the dump kickers (MKDs) to the tertiary collimators (TCT). The MKD-TCT phase advance determines the protected aperture in the horizontal plane [33], whereas in the vertical plane the protected aperture is limited by the cleaning efficiency [11]. All the constraints in IR6, as well as the different values of the alternative optics studied after phase optimisation, are summarized in Table 2.

Figure 16 shows the $\Delta\mu_{x,y}^{IP1-5}$ scan performed on the Baseline optics for Beam 1 and 2. The DA at each phase step is calculated after 10^6 turns and without non-linear field errors. The scan plot shows the average DA over 60 angles, as for the phase optimisation the DA is more sensitive to the $x-y$ angle and an increased sampling reduces the probability of missing a drop in DA. The impact of $\Delta\mu_{x,y}^{IP1-5}$ shift can be significant on the DA. While for Beam 1 the phase was close to an optimum, one had to extend the phase excursion in the case of Beam 2 to find an optimum DA comparable to Beam 1. By shifting the phase in Beam 1 by $\Delta\mu_x^{IP1-5} = +\pi/10$ and $\Delta\mu_y^{IP1-5} = +\pi/10$, one obtains an increase in

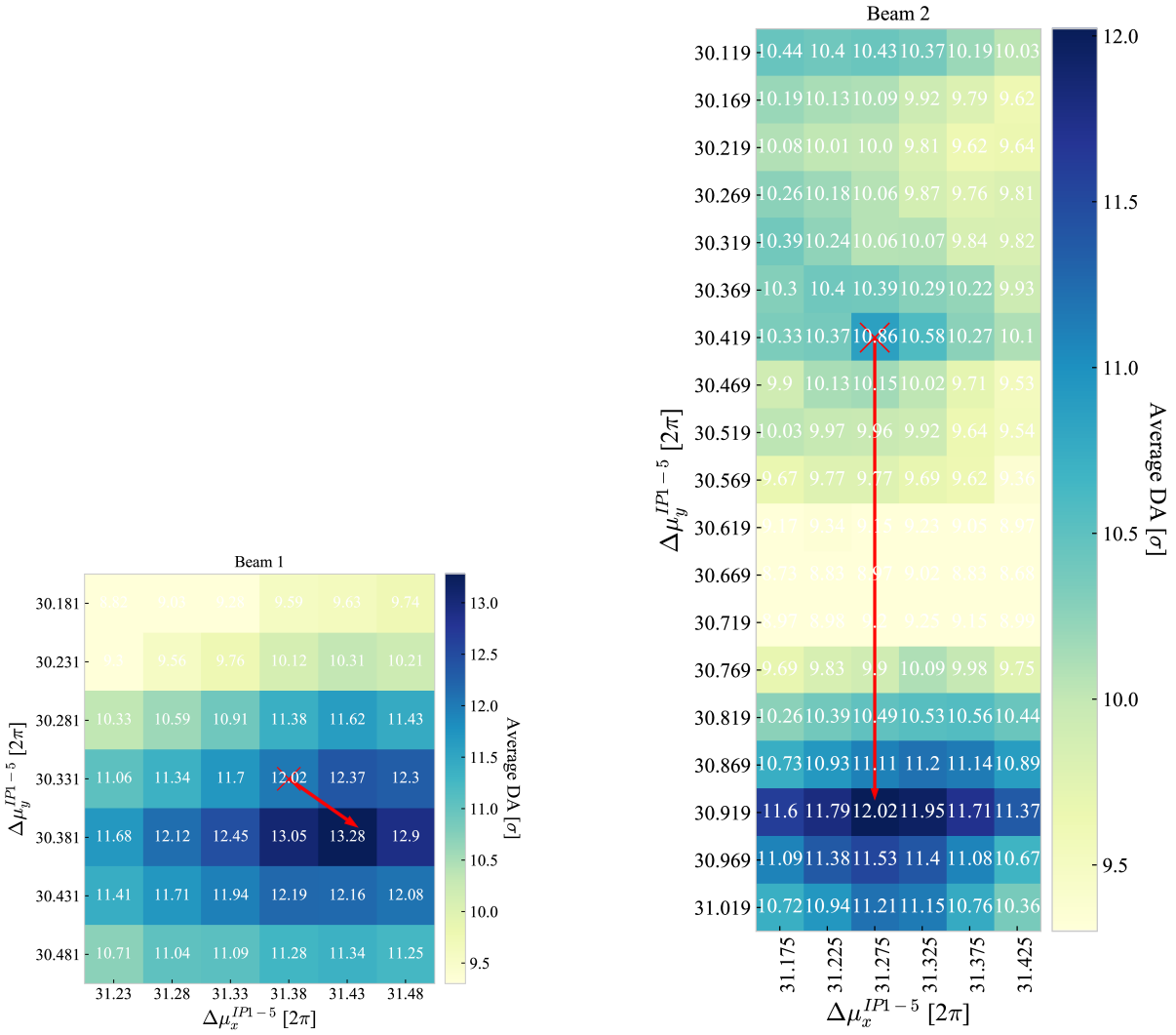

Fig. 16: $\Delta\mu_{x,y}^{IP1-5}$ scan as function of the average DA, on the Baseline optics for Beam 1 (left plot) and for Beam 2 (right plot). The DA is simulated with $I_{\mathrm{MO}} = -570$ A, crossing scheme and dispersion correction, Q' = 15, without non-linear field imperfection, over 60 angles and 10^6 turns. The red cross shows the original phase advance $\Delta\mu_{x,y}^{IP1-5}$ before optimisation, and the arrow the DA improvement. For Beam 2 the scan of the vertical phase advance (not limited by the MKD-TCT phase constraint) has been extended to find the optimal DA.

$\Delta\mathrm{DA}_{\mathrm{avg}}$ = +1.3 σ. For Beam 2, the phase have been shifted by $\Delta\mu_x^{IP1-5} = 0$ and $\Delta\mu_y^{IP1-5} = +\pi$, for an increase in $\Delta\mathrm{DA}_{\mathrm{avg}}$ = +1.16 σ. The scan performed on the No MS10 optics and the No MS14F & MS14D optics has shown that the optimal DA is obtained by applying almost the same phase shift as applied to the Baseline optics. For the No MS10 case, the DA has improved by $\Delta\mathrm{DA}_{\mathrm{avg}}$ = +1.4 σ for Beam 1 and $\Delta\mathrm{DA}_{\mathrm{avg}}$ = +0.5 σ for Beam 2. For the No MS14F & MS14D case, $\Delta\mathrm{DA}_{\mathrm{avg}}$ = +0.8 σ for Beam 1 and $\Delta\mathrm{DA}_{\mathrm{avg}}$ = +0.6 σ for Beam 2. However, for the No MS14F optics, due to the change in optics applied on the right side of IP1 and IP5 (see Section 3.1), the optimal phase setting is therefore very different from the other designs. It was noted previously (see Fig. 14), the large drop of DA for Beam 1 compared to Beam 2 for the No MS14F case. This can be partly explained by the bad phase $\Delta\mu_{x,y}^{IP1-5}$ setting in the case of Beam 1 as shown in Fig. 17. In that case, the maximum $\mathrm{DA}_{\mathrm{avg}}$ was found at μ_x^{IP1-5} = 31.625 and μ_y^{IP1-5} = 30.411 (in 2π units). However, the large shift of the horizontal phase advance required is incompatible with the MKD-TCT phase constraint, which has to be a value

Table 2: Comparison of the IR6 main parameters for the different proposed optics (after $\Delta\mu_{xy}^{IP1-5}$ optimisation).

Param. B1 / B2	Target values	Baseline	No MS14F	No MS14F & MS14D
$\Delta\mu_{x,\mathrm{MKD-TCDQ}}$ [°]	$90^\circ \pm 4^\circ$	86.3 / 93.6	91.5 / 93.6	86.3 / 93.6
β_y^{TCDS} [m]	≥ 200	238.3 / 260.6	283.2 / 200.0	238.3 / 271.0
β_x^{TCDQ} [m]	-	736.4 / 473.3	513.9 / 460.0	736.4 / 474.6
β_y^{TCDQ} [m]	$\geq$145	180.5 / 145.0	145.0 / 176.2	180.5 / 145.0
$\lvert D_{x,\mathrm{TCDQ}}\rvert$ [m]	-	0.6 / 0.4	0.02 / 0.38	0.5 / 0.42
$\mathrm{Gap}_{\mathrm{TCQD,min}}$ [mm]	$\geq$3	4.0 / 3.05	3.3 / 2.99	4.0 /3.05
β_x^{TDE} [km]	$\geq$4	6.37 / 4.92	5.06 / 4.83	6.37 / 4.93
β_y^{TDE} [km]	$\geq$3.2	3.36 / 7.23	8.2 / 6.33	3.36 / 7.72
$(\beta_x\beta_y)^{\frac{1}{2}}_{\mathrm{TDE}}$ [km]	$\geq$4.5	4.62 / 5.98	6.44 / 5.53	4.62 / 6.17
$\lvert\Delta\mu_{x,\mathrm{MKD-TCT,IP1}}\rvert$ [°]	$\leq$20	19.8 / 18.8	9.8 / 18.6	5.0 / 19.6
Q5.L6 [T/m]	160	163 / -164	160 / -162	163 / -165
Q5.R6 [T/m]	160	-159 / 151	-161 / 151	-159 / 152

below 20° (modulo π) for a protected aperture in the horizontal plane of about 11.2σ. Therefore, the scan was extended in the vertical plane and the best DA value was found by changing the phase by $\Delta\mu_x^{IP1-5} = +\pi/5$ and $\Delta\mu_y^{IP1-5} = +\pi$. For Beam 2, the original phase advance was already very close to the optimal value. Finally, the gain in DA for the optimal settings are $\Delta\mathrm{DA}_{\mathrm{avg}}$ = +1.9 σ for Beam 1 and $\Delta\mathrm{DA}_{\mathrm{avg}}$ = +0.2 σ for Beam 2. The phases between IP1 and IP5, before and after optimisation, for each sextupole scheme option are summarized in Table 3.

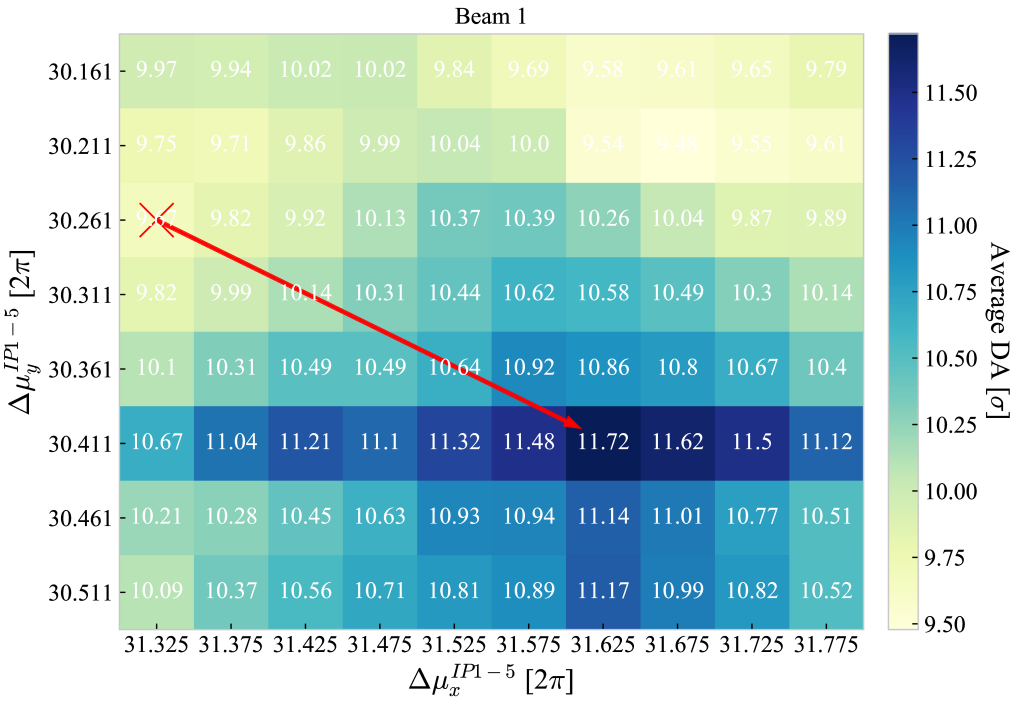

Fig. 17: $\Delta\mu_{x,y}^{IP1-5}$ scan as a function of the average DA, on the No MS14F optics (Beam 1).

It is worth mentioning the impact of the phase optimisation on the tune footprint on the different

Table 3: Phases between IP1 and IP5 before and after $\Delta\mu_{xy}^{IP1-5}$ optimisation

Optics	$\Delta\mu_x^{IP1-5}$ (B1/B2) [2π]	$\Delta\mu_y^{IP1-5}$ (B1/B2) [2π]
Before $\Delta\mu_{xy}^{IP1-5}$ optimisation		
Baseline	31.378 / 31.275	30.330 / 30.369
No MS10	31.378 / 31.275	30.330 / 30.369
No MS14F	31.325 / 31.308	30.261 / 30.371
No MS14F & MS14D	31.378 / 31.275	30.330 / 30.369
After $\Delta\mu_{xy}^{IP1-5}$ optimisation		
Baseline	31.430 / 31.275	30.381 / 30.919
No MS10	31.430 / 31.275	30.381 / 30.919
No MS14F	31.425 / 31.278	30.761 / 30.421
No MS14F & MS14D	31.380 / 31.275	30.380 / 30.919

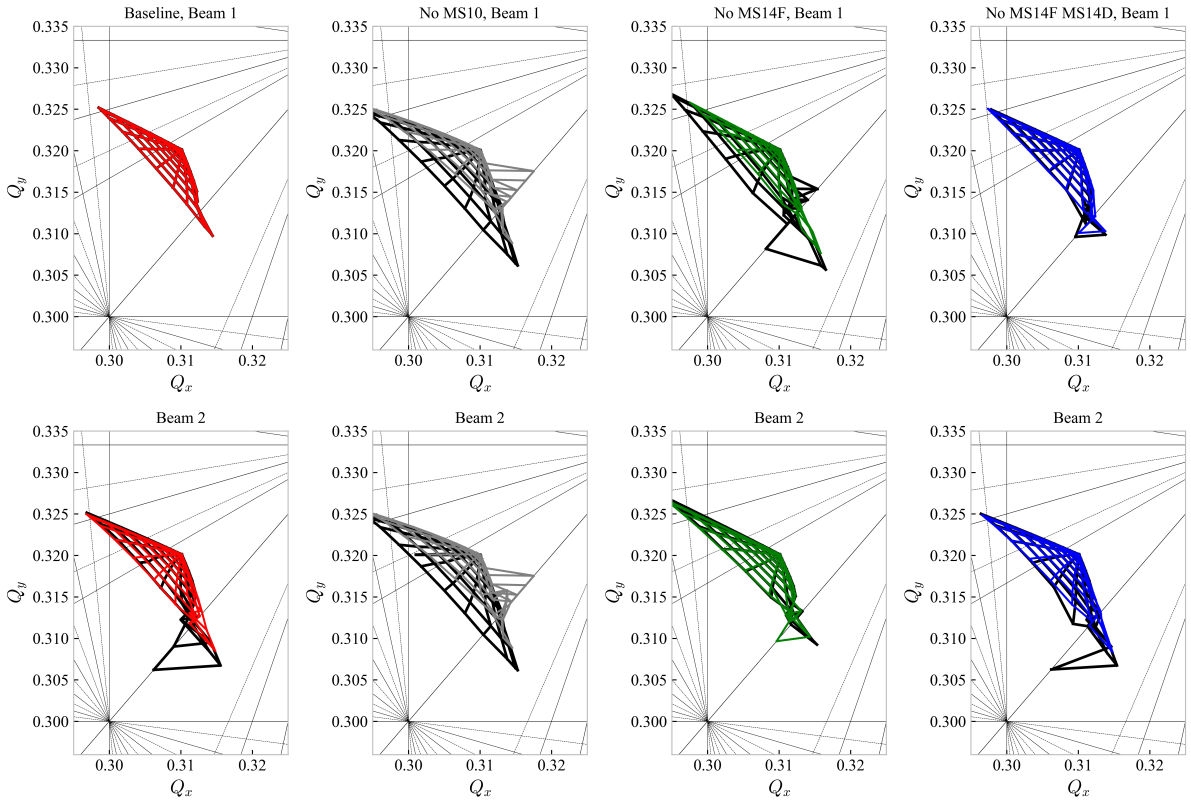

Fig. 18: Footprint on the tune diagram of the Baseline, No MS10, No MS14F and No MS14F & MS14D optics, tracked for particle amplitudes up to 10σ with $I_{\mathrm{MO}} = -570$ A, crossing scheme and dispersion correction, and $\delta_p = 0$. The black lines show the footprint before $\Delta\mu_{x,y}^{IP1-5}$ optimisation and the coloured lines after optimisation.

optics. The footprint in Fig. 18 was simulated by tracking on-momentum particles up to 10σ, using the MAD-X [34] tracking module. The optics configuration includes the beam crossing scheme, orbit bumps for dispersion correction and Landau octupoles set to their maximum strength. While the linear amplitude detuning terms before and after phase optimisation were kept almost unchanged, the size of the footprints were slightly reduced for all the cases, except for the Beam 1 of the No MS14F for which the footprint

significantly shrinks and for which the increase after phase optimisation was the most important. This indicates that mainly higher-order amplitude detuning terms were affected by the phase changes.

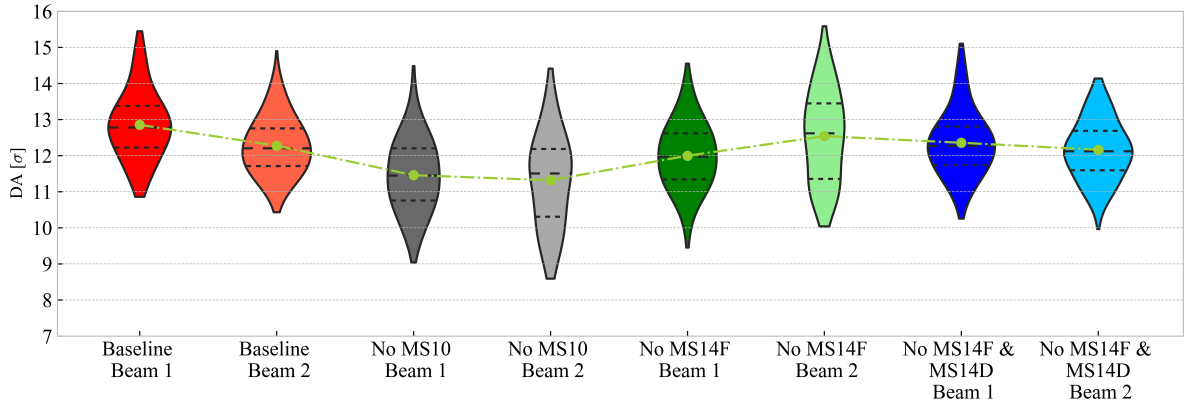

Fig. 19: Dynamic aperture comparison between all optics, with field imperfections, after $\Delta\mu_{x,y}^{IP1-5}$ phase optimisation and with Landau octupoles set to I_{MO} = -570 A.

When including non-linear field imperfections in the lattices, the DA of the optics with optimized phase advance $\Delta\mu_{x,y}^{IP1-5}$ is still well improved. Figure 19 shows the DA simulated after optimisation for 60 seeds, over 7 angles for 10^5 turns. For the Baseline, the average and minimum DA difference compared to the DA before phase optimisation has increased by $\Delta DA_{avg/min}$ = +1.0/+1.1 σ for Beam 1 and $\Delta DA_{avg/min}$ = +0.5/+0.9 σ for Beam 2. For the No MS10 optics, $\Delta DA_{avg/min}$ = +0.55/+1.4 σ for Beam 1 and $\Delta DA_{avg/min}$ = +0.5/+0.5 σ for Beam 2. For the No MS14F optics, $\Delta DA_{avg/min}$ = +1.0/+0.45 σ for Beam 1 and $\Delta DA_{avg/min}$ = +0/+0 σ for Beam 2. Finally, for the No MS14F & MS14D case, $\Delta DA_{avg/min}$ = +0.5/+1.0 σ for Beam 1 and $\Delta DA_{avg/min}$ = +0.3/- 0.2 σ for Beam 2. The DA before and after phase optimisation are summarized in Table 4. It could be possible to further improve the DA of the different optics by scanning the phase while including non-linear field imperfections for the DA calculation, as studied in [32], or by implementing online $\Delta\mu_{x,y}^{IP1-5}$ optics knobs to control the beam lifetime during operation.

Table 4: DA comparison for Beam 1 and 2 for the original optics with field imperfections before and after $\Delta\mu_{xy}^{IP1-5}$ optimisation.

Optics	Average DA (B1/B2) [σ]	Minimum DA (B1/B2) [σ]
Before $\Delta\mu_{xy}^{IP1-5}$ optimisation		
Baseline	11.9 / 12.0	9.7 / 9.5
No MS10	10.9 / 10.8	7.6 / 8.1
No MS14F	11.1 / 12.5	9.0 / 10.1
No MS14F & MS14D	11.9 / 11.9	9.3 / 10.2
After $\Delta\mu_{xy}^{IP1-5}$ optimisation		
Baseline	12.9 / 12.3	10.9 / 10.4
No MS10	11.5 / 11.3	9.0 / 8.6
No MS14F	12.0 / 12.5	9.5 / 10.1
No MS14F & MS14D	12.4 / 12.2	10.3 / 10.0

4 DA studies with beam-beam interactions for the proposed optics scenarios

To validate the different sextupole scheme scenarios studied so far, it is crucial to include performance limitations resulting from beam-beam interactions. In the following study, only the incoherent, or weak-strong effects, are included in the tracking simulations, as they are more likely to create resonances causing particle losses and emittance growth [35], than the strong-strong (coherent) effects.

Regarding the simulation framework, the tracking is done using SixTrack and the SixDesk environment. A single beam is tracked in the potential generated by the other with static beam-beam lenses [36]. The present DA studies will help to identify the optimal sextupole configuration as well as the possible optimum tune working points (WP) for operation at collision. For the DA calculation, the particles were tracked for 10^6 turns, their amplitudes distributed over 5 angles, and no field imperfections were included. Based on extensive past DA studies and their correlation to beam lifetime [37], the target minimum DA for a robust HL–LHC design is 6σ. In Figure 20, a working point (WP) optimisation is performed at collision with the octupoles fully powered, half crossing angle of 295μrad and the DA scans are compared before and after $\Delta\mu_{xy}^{IP1-5}$ phase optimisation for each sextupole scheme option, for Beam 1. The bunch population corresponds to the beam intensity at the end of the levelling process, $\approx 1.2\times10^{11}$ protons per bunch (ppb) for the operation at maximum levelled luminosity of $5 \times 10^{34}\mathrm{cm}^{-2}\mathrm{s}^{-1}$.

For the Baseline scenario, the phase optimisation of this optics does not improve the available tune space above the 6 σ target. However, both lattices provide a large tune area above the target and a clear WP area with DA above 7 σ. It is worth noticing that this WP is close to the coupling resonance lines. While some coupling is generated from the feed-down to skew quadrupole field generated by the vertical orbit bumps at the strong sextupoles, additional linear coupling is expected when considering lattice imperfections and may alter the value of the optimal WP.

For the No MS10 scenario, there is a comfortable WP area above the 6 σ DA target, although reduced compared to the Baseline, before and after $\Delta\mu_{xy}^{IP1-5}$ phase optimisation. After phase optimisation, one can observe a sizeable improvement of the DA scan. Despite the large geometrical aberrations generated, the tune scan performed on the No MS10 optics, suggests that this option can be a viable solution for HL–LHC.

The solution of bypassing the MS14F can be envisaged only after tuning the $\Delta\mu_{xy}^{IP1-5}$ phase advance. In this case, the DA is significantly improved with a large available tune area above the target. A safe option is the No MS14F & MS14D optics, where the target is reached before and after phase optimisation, similarly to the Baseline optics. These simulations have been performed assuming a half angle at IP1 and IP5 of 295μm. However, recent update on the operational scenario for HL–LHC converge towards a smaller half crossing angle of 250μm which increase the impact of beam-beam long-range on the DA. Figure 21 shows the impact on the tune scan with beam-beam, before and after phase optimisation, for the No MS10 option. This study shows that considering the current operational scenario parameters, keeping the LHC sextupole configuration can be a feasible solution for HL–LHC, but only after a careful tuning of the phase advance between IP1 and IP5.

5 Octupole powering optimisation

The Landau octupoles, required in the HL–LHC for beam stability, are also a large source of non-linear resonances that can degrade the beam lifetime. Those resonances are essentially generated in the neighbouring sectors of the low-β^* interaction points IP1 and IP5. Also, the large orbit bumps needed in these regions for horizontal and vertical dispersion correction induce strong feed-down to normal and skew sextupole RDTs from the beam offset at the octupoles. In this study, one explores the possibility of improving the DA by minimizing the RDTs generated by the octupoles while keeping equivalent linear amplitude detuning for Landau damping. The present octupole powering strategy for HL–LHC at collision is to power all the magnets with equal strength and negative polarity (currently under review [38]). Assuming the option of powering all the octupoles to -300 A, corresponding to the minimum required for

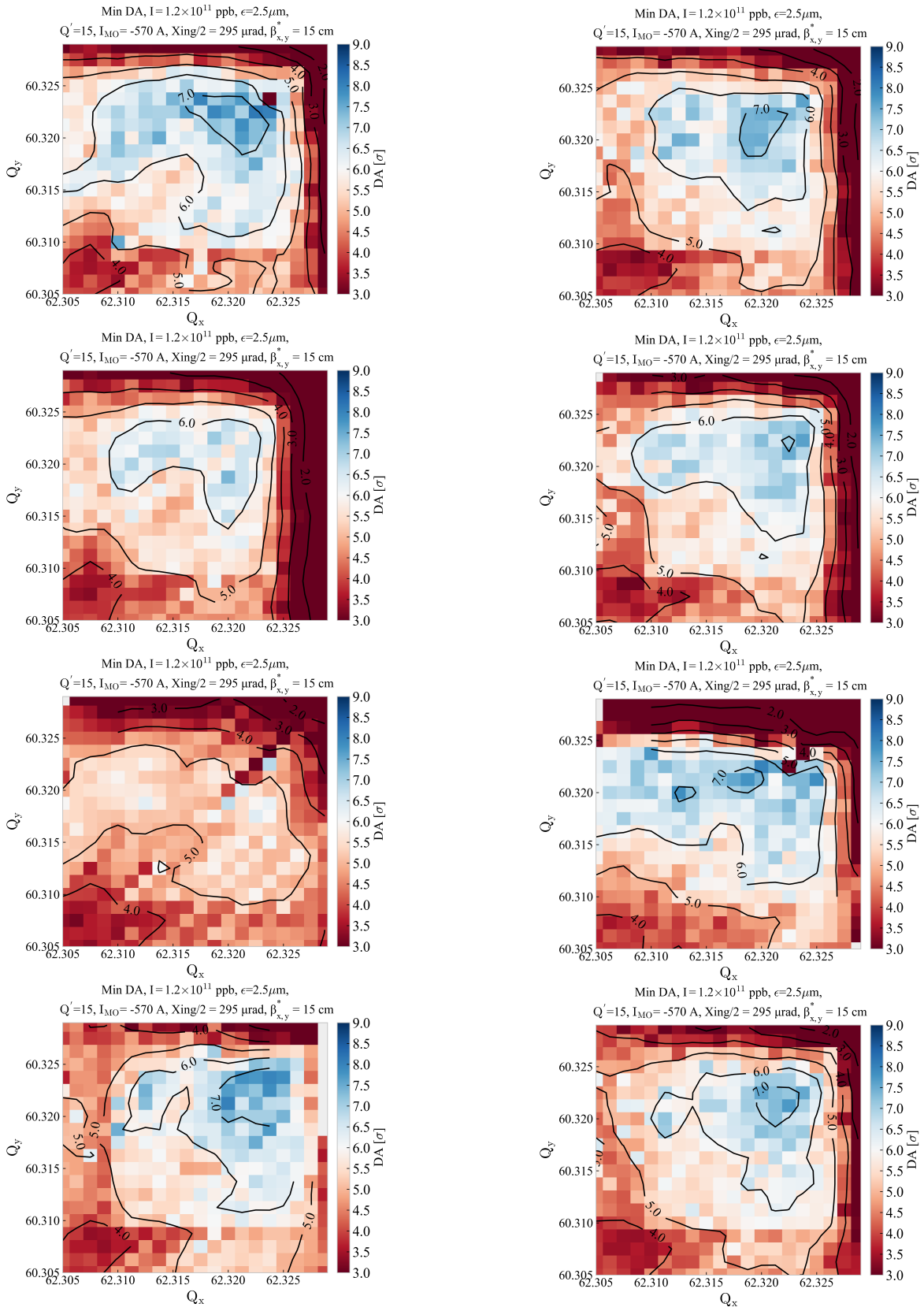

Fig. 20: Scan of the horizontal and vertical tunes before (left) and after (right) phase advance optimisation between IP1 and IP5 for Beam 1 for the Baseline, No MS10, No MS14F, and No MS14F & MS14D optics (top to bottom) .

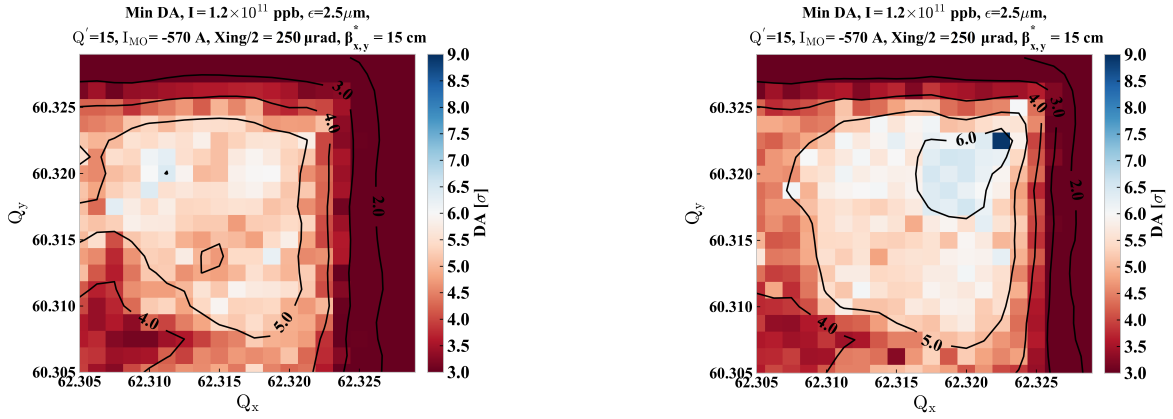

Fig. 21: Scan of the horizontal and vertical tunes before (left) and after (right) phase advance optimisation between IP1 and IP5 for Beam 1 for the No MS10 optics, with a reduced half crossing angle at IP1 and IP5 of 250μm.

coherent stability [23], one can therefore reduce or increase the octupole strengths in particular sectors while keeping the effective tune spread constant. It is worth noting that, if during operation the machine requires the full power of the octupoles at collision, the powering optimisation described here cannot be applied.

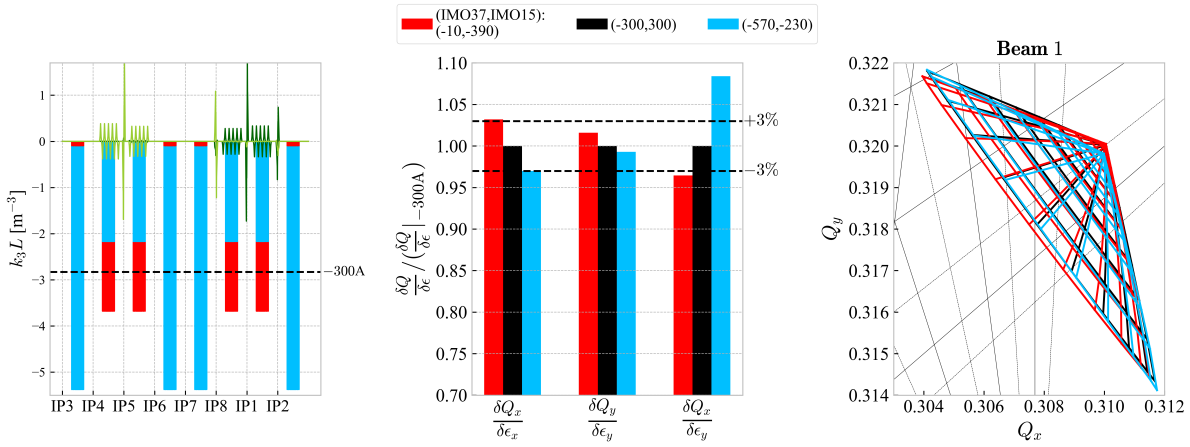

Fig. 22: Left: Octupole powering schemes (black, blue and red lines) and orbit bumps for the crossing scheme and dispersion correction. Middle: Linear amplitude detuning terms normalized to the values expected with equal powering of the octupoles at -300 A. Right: Footprint for on-momentum beam. The strength of the octupoles in sectors (23,34,67,78) is referred to as IMO37 and in sectors (81,12,45,56) as IMO15. Simulated on the Baseline optics (Beam 1).

The strategy applied here, was reducing the octupole current in the sectors involved in the ATS squeeze where the large dispersion correction bumps are located and to compensate the missing strength by increasing the current in the other sectors. As the β-functions in the ATS sectors are much larger than in the rest of the ring, a reduction of $\sim$70 A in sectors 81, 12, 45, 56, requires an increase of $\sim$170 A for the octupoles in sectors 23, 34, 67, 78 to keep the direct linear amplitude detuning terms almost constant. Figure 22 shows as example three different octupole powering strategies with equal strength for all magnets (black lines), reduced (blue lines) and increased (red lines) current in ATS sectors and their corresponding linear amplitude detuning values and tune footprints. Here the target is to keep the

direct terms within a $\pm 3\%$ margin, which results in a tiny change in the tune diagram.

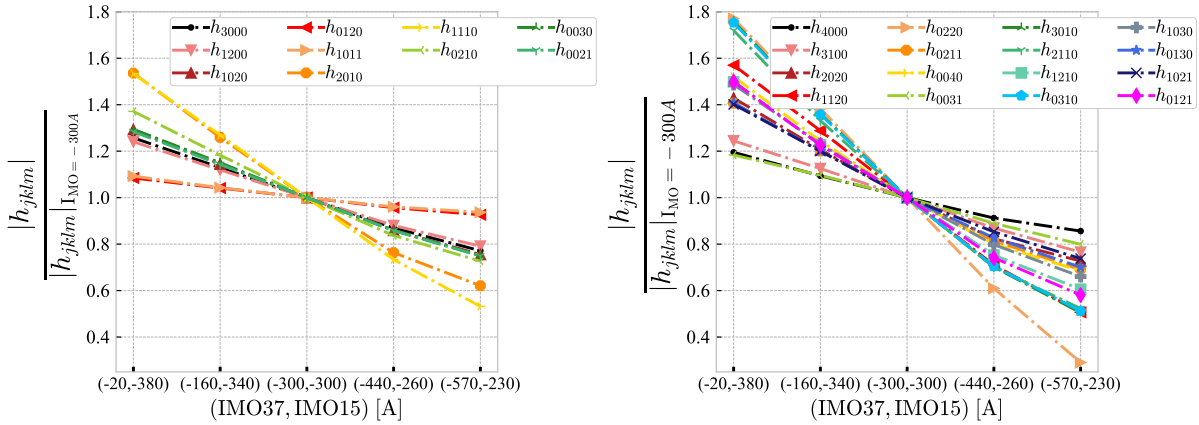

Fig. 23: Average normal and skew sextupole (left plot) and octupole (right plot) RDTs, as a function of different octupole powering between IMO37 and IMO15 for the Baseline optics (Beam 1). The RDTs are normalized to the corresponding average value when all octupole are equally powered at -300 A, and computed using PTC.

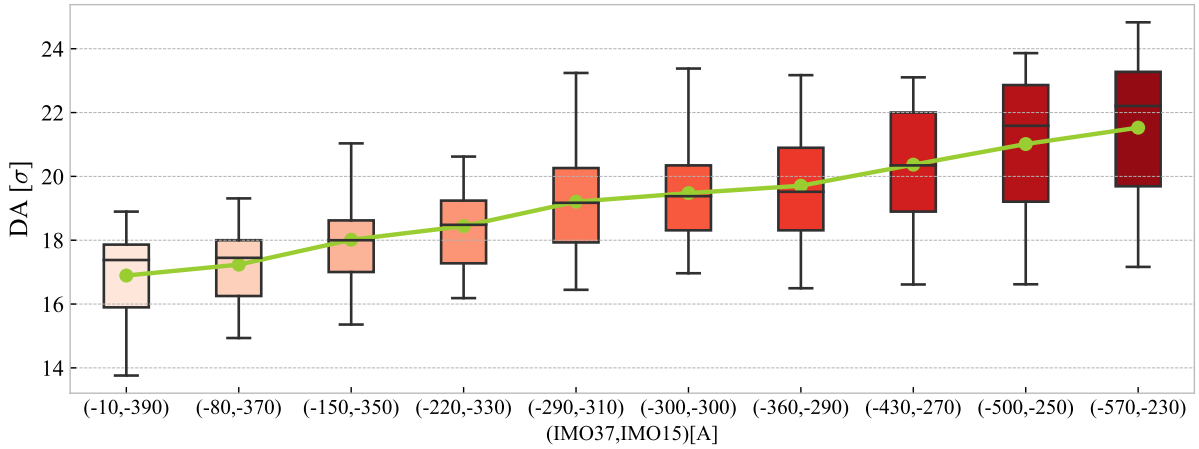

Fig. 24: Statistical DA distribution as a function of octupole (IMO37,IMO15) powering for the Baseline optics (Beam 1). The coloured box shows the interquartile range, the middle black line the median value and the bars at the extremities the min/max DA.

Figure 23 shows the clear dependence of the octupolar and sextupolar RDTs generated in the machine and the octupole current in the arcs adjacent to IP1 and IP5. Relaxing the current in those regions allows reducing sextupole and octupole geometrical aberrations and potentially also higher-order resonances. The same dependence has been observed for all the different sextupole schemes. In Fig. 24 the DA is computed for different octupole powering with constant direct amplitude detuning terms. The DA was simulated without imperfections with amplitudes distributed over 60 angles and tracked for 10^6 turns. While reducing the octupole current IMO15 to -230 A shows only a tiny improvement of the minimum DA, the average DA, however, has increased by ΔDA_{avg} = +2.2 σ compared to the DA computed with all octupoles powered equally at -300 A. Finally the impact on DA was checked including beam-beam interactions and the results are shown in Fig. 25 for the Baseline (top), No MS14F (middle), and No MS14F & MS14D (bottom) schemes with a reduced crossing angle at IP1 and IP5 of 250μm. The tune scans show that the minimum DA does not necessarily increase when reducing IM015, however the available tune space with DA above 6σ was enlarged in all cases.

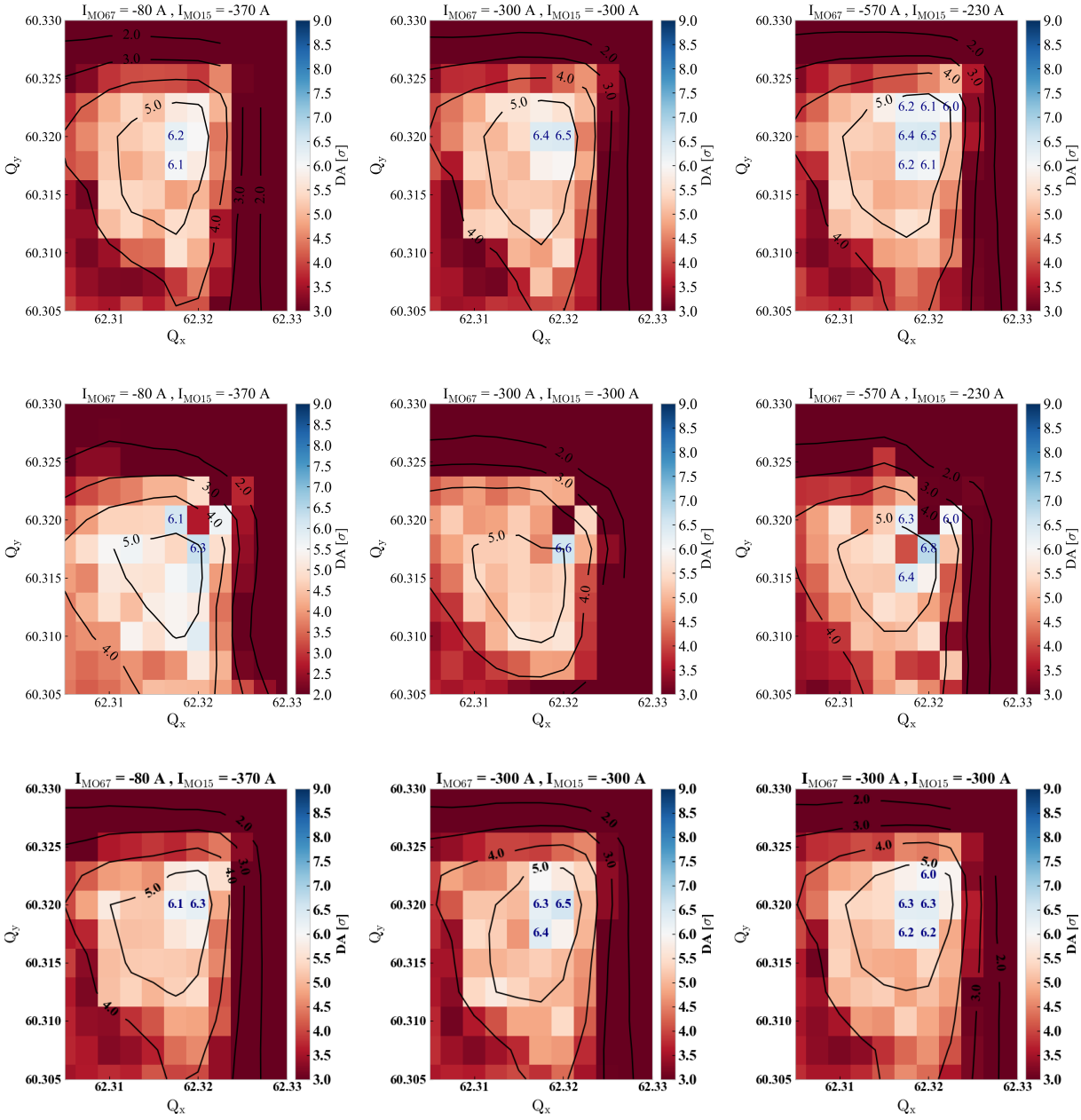

Fig. 25: Scan of the horizontal and vertical tunes after phase $\Delta\mu_{xy}^{IP1-5}$ optimisation for Beam 1 and for different octupole powering with constant linear amplitude detuning. Minimum DA computed including beam-beam interactions. The results are shown for the Baseline (top), No MS14F optics (middle), and No MS14F & MS14D optics (bottom) with a reduced half crossing angle at IP1 and IP5 of 250μm.

It would be possible to further optimize the DA by balancing the amount of normal or skew sextupolar RDTs generated. Indeed, the HL–LHC foresees to collide the beams in IP1 with a crossing angle in the horizontal plane, and in the vertical plane for IP5. Therefore, in sectors 81,12, the horizontal orbit bumps needed for dispersion correction will induce feed-down to skew sextupole field at the octupoles in this region, and normal sextupole field from the vertical offset at the octupoles in sectors 45,56. Adjusting independently the octupole current in the ATS sectors of IR1 and IR5 can allow reducing the amplitude of resonances that have larger impact on the DA.

6 Conclusions

The report has gathered simulation results that help to understand the mechanism behind DA reduction through the study of non-linear resonances resulting from different sextupole schemes or octupole powering. Extensive particle tracking campaigns have been carried out to optimize and verify the DA for different optics and sextupole schemes proposed for the HL–LHC design. The optimisation process included the effect of the magnet non-linear field errors estimated for HL–LHC, the weak-strong beam-beam interactions and also the various optics constraints imposed by the experiments or machine protection. The main goal of this study was to assess whether the installation of 8 new superconducting sextupoles (4 MS10 per beam), which is part of the baseline design, could be avoided by a clever optics design, while keeping the DA to a viable level for operation.

The additional MS10s are foreseen to restore the pairing of the strong sextupoles around IP1 and IP5 to allow the self-compensation of the geometrical aberrations generated by these magnets. It has been shown that these resonances in the presence of high telescopic factor have a sizeable impact on the DA and need to be corrected. Two alternative sextupole schemes are proposed here. For the first option, the focusing magnet MS14F is disconnected on the left side of IP1 and IP5 and the vertical betatron phase advance is shifted by $-\pi/2$ on the right side. For the second option, the focusing magnet MS14F is disconnected on the left side and the defocusing magnet MS14D is disconnected on the right side. Both options allow similar compensation of the sextupolar geometrical resonances as for the baseline. After tuning of the phase advance between IP1 and IP5 to optimize the DA, both alternative optics show a DA close to the baseline when field imperfections are included. The study has shown that after phase optimisation, tune space with a minimum DA above 6σ can be found, when beam-beam interactions are included, for all proposed scenarios (see Table 5). The optics and performance studies carried out on these new sextupole schemes, show that they can be realistic alternatives for the operation of the HL–LHC, at the cost of freezing the phase advance between IP1 and IP5, which is not desirable at this stage of the project. The No MS14F & MS14D optics is a more robust option to assure long-term stability of the beam. The drawback of this option is the larger chromatic β-beating, for which there are no clear requirements. This can, however, be reduced to similar level as the Baseline option by increasing the current from 90% to 95% of the ultimate strength of the defocusing strong sextupoles on the right side of IR1. Furthermore, the DA scan studies have shown that the option of the LHC-like sextupole lattice (No MS10) could achieve the desired DA target if the $\Delta\mu_{xy}^{IP1-5}$ phase advance is well optimized.

Assuming that the octupole current required for stability allows enough margin, it has been shown that reducing the weight on the octupole strength in the ATS sectors, allow reducing significantly the resonances that are partially responsible for DA degradation. A clear correlation between the octupole and feed-down to sextupole RDTs generated in these regions and the DA has been established. RDTs of different nature are generated in the two ATS regions. Large horizontal bumps are crossing the octupoles in sectors 45,56 while vertical bumps are created in sectors 81,12, resulting in feed-down to normal and skew sextupole fields, respectively. Therefore, further DA improvement can be achieved by optimizing the weights put on octupole current in these sectors.

The study has been carried out for the most demanding configuration ($\beta^* = 15\mathrm{cm}$) of the present baseline scenario. Flat optics are expected to exacerbate the issue due to the larger telescopic factor, while optics will smaller telescopic factors will be less affected. Further analysis will be required to assess the robustness and feasibility of the proposed mitigation strategies. Run 4, initially targeting a round optics of $\beta^* = 20\mathrm{cm}$ [39] would not strictly require the installation of the additional MS10. However, in case lower β^* and/or flat optics would be needed (for instance to compensate for low bunch population or difficulties in controlling crab cavity main mode), the impact of not installing the MS10 needs to be re-evaluated.

Table 5: Summary comparison table of the key parameters between the different sextupole lattice options for HL-LHC after phase optimisation between IP1 and IP5 (compatible with IR6 constraints).

Parameters	Baseline	No MS10	No MS14F	No MS14F & MS14D
$\Delta\mu_x^{IP1-5}$ B1/B2 [2π]	31.430 / 31.275	31.378 / 31.275	31.425 / 31.278	31.380 / 31.275
$\Delta\mu_y^{IP1-5}$ B1/B2 [2π]	30.381 / 30.919	30.330 / 30.369	30.761 / 30.421	30.381 / 30.919
Q_x/ϵ_x (MO = -570 A) B1/B2 [10^5m^{-1}]	-3.69 / -4.10	-3.56 / -3.81	-3.95 / -4.21	-3.91 / -4.24
Q_y/ϵ_y (MO = -570 A) B1/B2 [10^5m^{-1}]	-3.33 / -3.35	-3.21 / -3.27	-3.41 / -3.37	-3.35 / -3.39
Q_x/ϵ_y (MO = -570 A) B1/B2 [10^5m^{-1}]	1.59 / 1.64	1.55 / 1.75	1.85 / 1.85	1.59 / 1.61
Horizontal chrom. β-beating IP **1**/2/**5**/8 IP 3/4/6/7 δ_p=3×10^{-4} (Beam 1) [%]	**0.6**/0.005/**1.0**/1.7 0.9/0.4/1.8/1.1	**0.8**/0.003/**1.3**/1.7 0.9/0.3/1.2/1.5	**0.2**/0.3/**1.8**/0.8 1.5/2.0/1.8/2.4	**0.1**/0.5/**0.9**/2.2 1.2/1.0/0.5/2.2
Vertical chrom. β-beating IP **1**/2/**5**/8 IP 3/4/6/7 δ_p=3×10^{-4} (Beam 1) [%]	**0.3**/0.7/**0.8**/1.9 0.7/0.5/2.4/0.2	**1.4**/2.3/**2.5**/2.2 2.4/1.4/3.6/3.0	**2.3**/0.08/**0.5**/2.7 0.3/0.8/3.0/4.2	**3.7**/4.0/**4.6**/2.8 4.2/1.0/6.4/5.8
Average DA (B1/B2) 60 seeds, 10^5 turns, with field imperfections, MO=-570 A Q'=15, Xing = 295 μrad [σ]	**12.9 / 12.3**	**11.5 / 11.3**	**12.0 / 12.5**	**12.4 / 12.2**
Minimum DA (B1/B2) 60 seeds, 10^5 turns, with field imperfections, MO=-570 A Q'=15, Xing = 295 μrad [σ]	**10.9 / 10.4**	**9.0 / 8.6**	**9.5 / 10.1**	**10.3 / 10.0**

7 Acknowledgements

We would like to thank F. Van der Veken, N. Karastathis and S. Kostoglou for the precious help for the dynamic aperture and frequency map analysis simulations setup. We would like to acknowledge G. Arduini, X. Buffat, R. Bruce, S. Fartoukh, and R. Tomás for very useful comments and discussions that helped us guide our studies.

References

[1] G. Apollinari, I. Bejar Alonso, and O. Bruning. High-luminosity large hadron collider (HL-LHC): TDR V.0.1. Technical Report CERN-2017-007-M, CERN, 2017.

[2] S. Fartoukh. Achromatic telescopic squeeze and application to the lhc and its luminosity upgrade. *Physical Review Special Topics - Accelerators and Beams*, 16(11102), 2013.

[3] R. De Maria and S. Fartoukh. SLHCV3.0: layout, optics and long term stability. Technical Report sLHC-PROJECT-REPORT-0050, CERN, 2010.

[4] R. De Maria, S. Fartoukh, and M. Giovannozzi. Review of Q5 in IR6 and MS10 in IR1-5. Presented at the 12th HL-LHC Parameter and Lay-out Committee meeting, CERN, 14/10/2014. `https://indico.cern.ch/event/340523/`.

[5] R. De Maria, F. Van der Veken, and M. Giovannozzi. New optics layout (v1.3) and possible simplifications (MS10). Presented at the 7th HL-LHC annual meeting, Madrid, 14/11/2017. `https://indico.cern.ch/event/647714/`.

[6] R. De Maria, S. D. Fartoukh, A. V. Bogomyagkov, and M. Korostelev. HLLHCV1.0: HL-LHC layout and optics models for 150 mm Nb3Sn triplets and local crab-cavities. In *Proceedings of IPAC13*, 2013.

[7] R. De Maria, S. D. Fartoukh, and M. Fitterer. HLLHCV1.1 optics version for the HL-LHC upgrade. In *Proceedings of IPAC15*, 2015.

[8] R. Bruce, N. Fuster-Martínez, A. Mereghetti, D. Mirarchi, and S. Redaelli. Review of LHC Run 2 machine configurations. In *Proceedings of 9th LHC Operations Evian Workshop, CERN-ACC-2019-059*, 2019.

[9] R. Tomas et al. LHC run 2 optics commissioning experience in view of HL-LHC. In *Proceedings of IPAC19*, 2019.

[10] X. Buffat et al. Transverse instabilities. In *Proceedings of 9th LHC Operations Evian Workshop*, 2019.

[11] R. De Maria, R. Bruce, D. Gamba, M. Giovannozzi, and F. Plassard. HL-LHC optics and layout HLLHCV1.4. In *Proceedings of IPAC 2019*, 2019.

[12] R. De Maria et al. HL-LHC optics version v1.4. 58th HL-LHC TCC meeting, CERN, 20/10/2018, 2018. `https://indico.cern.ch/event/758028`.

[13] R. De Maria et al. HLLHCV1.4 optics repository. `http://lhc-optics.web.cern.ch/lhc-optics/HLLHCV1.4/`.

[14] Lifetrac manual. `https://cdcvs.fnal.gov/redmine/projects/lifetrac/wiki/FMA_Analysis`.

[15] E. Forest, F. Schmidt, and E. Mcintosh. Introduction to the Polymorphic Tracking Code. Technical Report CERN-SL-2002-044 / KEK 2002-03, CERN, KEK, 2002.

[16] L. Deniau, A. Latina, T. Persson, I. Shreyber, P. Skowronski, H. Burkhardt, R. De Maria, M. Giovannozzi, M. Jowett, J., F. Schmidt, and T. Glassle. Upgrade of MAD-X for HL-LHC project and FCC studies. In *Proceedings for ICAP 2018*, 2002.

[17] Y. Papaphilippou. Detecting chaos in particle accelerators through the frequency map analysis method. *Chaos*, 24(arXiv:1406.1545):024412. 29 p, Jun 2014.

[18] F. Schmidt. SixTrack - Version 4.2.16 - Single Particle Tracking Code Treating Transverse Motion with Synchrotron Oscillations in a Symplectic Manner - User Reference Manual. Technical Report CERN/SL/94-56(AP), CERN, 2012.

[19] SixTrack web site. `http://cern.ch/sixtrack/`.

[20] E. McIntosh and R. De Maria. The sixdesk run environment for SixTrack. Technical Report CERN-ATS-Note-2012-089 TECH, CERN, 2012.

[21] R. Bruce, C. Bracco, R. De Maria, M. Giovannozzi, S. Redaelli, R. Tomas, F. Velotti, and J. Wen-

ninger. Parameters for HL-LHC aperture calculations. Technical Report CERN-ACC-2014-0044, CERN, 2014.

[22] R. Bruce, C. Bracco, R. De Maria, M. Giovannozzi, S. Redaelli, R. Tomas, F. Velotti, and J. Wenninger. Updated parameters for HL-LHC aperture calculations for proton beams. Technical Report CERN-ACC-2017-0051, CERN, 2017.

[23] E. Metral et al. Update of the HL-LHC operational scenarios for proton operation. Technical Report CERN-ACC-NOTE-2018-0002, CERN, 2018.

[24] F. Plassard. No ms10 studies. 158th HiLumi WP2 Meeting, CERN, 10/9/2019, 2019. https://indico.cern.ch/event/844767/contributions/3546870.

[25] E. Todesco. Field quality tables: October 2015. https://espace.cern.ch/HiLumi/WP3/SitePages/Home.aspx.

[26] F. Plassard. Possibility to suppress the installation of MS in Q10 in IR1 and IR5. 144th HiLumi WP2 Meeting, CERN, 19/3/2019, 2019. http://indico.cern.ch/event/803396/contributions/3340845/.

[27] F. Plassard and R. De Maria. Hl-lhc v1.3 optics repository. /afs/cern.ch/eng/lhc/optics/HLLHCV1.3/squeeze2_ms14f/.

[28] X. Buffat et al. Strategy for landau damping of head-tail instabilities at top energy in the HL-LHC. Technical Report CERN-ACC-NOTE-2020-0059, CERN, 2020.

[29] J. Bengtsson. The sextupole scheme for the Swiss Light Source (SLS): an analytical approach. Technical Report SLS Note 9/97, BNL, 1997.

[30] S. Redaelli. Beam cleaning and collimation systems. In *Proceedings of the Joint International Accelerator School*, 2016. CERN-2016-002.

[31] G. Apollinari, I. Bejar Alonso, and Bruning O. Collimation system (Chapter 5). In *HL-LHC TDR V.0.1,*, 2017. CERN-2017-007-M.

[32] Y. Cai, R. De Maria, M. Giovannozzi, Y. Nosochkov, and F. Van der Veken. Dynamic aperture studies for HL-LHC V1.0. Technical Report CERN-ACC-2018-0054, CERN, 2018.

[33] R. Bruce and S. Redaelli. Protected aperture in HL-LHC. https://indico.cern.ch/event/668031.

[34] MAD-X web site. http://cern.ch/mad/.

[35] N. Karastathis, R. De Maria, S. Fartoukh, Y. Papaphilippou, and D. Pellegrini. Refining the HL-LHC Operational Settings with Inputs From Dynamic Aperture Simulations: A Progress Report. *J. Phys. : Conf. Ser.*, 1067(CERN-ACC-2018-124.2), 2018.

[36] K Hirata, Herbert W Moshammer, and F Ruggiero. A symplectic beam-beam interaction with energy change. *Part. Accel.*, 40(KEK-92-117):205–228. 25 p, Sep 1992.

[37] Papaphilippou Y et al. Long range beam-beam effects for HL-LHC. LHC Performance Workshop 2018 (Chamonix, France). https://indico.cern.ch/event/676124.

[38] X. Buffat. An update on HL-LHC octupole requirement. 170th HiLumi WP2 Meeting, CERN, 10/3/2020. https://indico.cern.ch/event/881273/.

[39] R. Tomas. Proton performance and ramp-up scenarios. 10th HL-LHC Collaboration Meeting, CERN, 7/10/202. https://indico.cern.ch/event/937797/.